Alma Mater Studiorum - Università di Bologna

SCUOLA DI SCIENZE

Dipartimento di Chimica Industriale"Toso Montanari"

Corso di Laurea Magistrale in

Chimica Industriale

Classe LM-71 - Scienze e Tecnologie della Chimica Industriale

Study of the effectiveness of crystal growth modifiers in the prevention of damage due to crystallization of sodium carbonates in stone artworks

Tesi di laurea sperimentale

CANDIDATO

Laura Samperisi

RELATORE

Chiar.mo Prof. Elena Bernardi

CORRELATORE

Prof. Carlos Manuel Rodríguez Navarro

Anno Accademico 2017-2018

A due occhi azzurri
ed un bicchiere di buon vino

Contents

Abstract

The disintegration of stone materials used in sculpture and architecture due to the crystallization of salts is capable of irreparably damaging artistic objects and historic buildings. Numerous conservation treatments have been proposed to prevent salt weathering or to ameliorate its effects. Among them, the use of crystallization modifiers have been proposed as a novel treatment for either inhibit salt crystallization and induce the formation of harmless efflorescence (that facilitate desalination) or to promote salt crystallization at very low supersaturation, thus preventing damage by reducing the effective crystallization pressure exerted by salts within porous materials such as stone, mortars or bricks. A number of phosphonates and carboxylates were tested here as potential crystallization modifiers for sodium carbonate crystallization. Precipitated phases during crystallization induced either by cooling or by evaporation tests were nahcolite ($NaHCO_3$), natron ($Na_2CO_3 \cdot 10H_2O$) and thermonatrite ($Na_2CO_3 \cdot H_2O$), identified using X-ray diffraction (XRD). By using the thermodynamic code PHREEQC and the calculation of the nucleation rate it was demonstrated that nahcolite had to be first phase formed during both tests. The formation of the other phases depended on the experimental conditions under which the two tests were conducted. Nahcolite nucleation is strongly inhibited in the presence of sodium citrate tribasic dihydrate (CA), polyacrylic acid 2100MW (PA) and etidronic acid (HEDP), when the additives are dosed at appropriate concentrations and the pH range of the resulting solution is about 8. Electrostatic attraction generated between the deprotonated organic additives and the cations present in solution or in pre- nucleation clusters appears to be the principal mechanism of additive-nahcolite interaction. Salt weathering tests, in addition to mercury intrusion porosimetry tests allowed to quantify the damage induced by such salts and determine where they were precipitating within porous limestone. FESEM observation of both salts grown on calcite single crystals and in limestone blocks subjected to salt crystallization tests allowed to identify how these additives inhibit nahcolite crystallization and their effect on crystal growth and development. The results show that PA seems to be the best inhibitor, while CA and HEDP, which show similar behaviors, are slightly less effective. The use of such effective crystallization inhibitors may lead to more efficient preventive conservation of ornamental stone affected by crystallization damage due to formation of sodium carbonate crystals.

1. Introduction and purpose

The disintegration of stone materials used in sculpture and architecture due to the crystallization of salts has serious economic effects and is capable of irreparably damaging artistic objects and historic buildings. Therefore, it is important to look for solutions that prevent or reduce the damage due to this phenomenon.

Many methods have been developed to avoid or minimize damage due to the crystallization of salts in the pores of ornamental rocks, almost all with little success. As the crystallization pressure is the most important parameter in salt weathering [1], treatments can be proposed to modify or reduce the deleterious effects of this damage mechanism at its origins.

In the last 17 years, the use of additives (inhibitors or crystallization promoters) has been proposed to modify the crystallization process, avoiding or reducing damage to the substrate in which the salt precipitates compared to those caused in the absence of additives [2; 3; 4; 5; 6].

Any foreign substance other than the compound that crystallizes is considered as an additive or impurity. Certain molecules or ions have the ability to inhibit and/or promote crystal growth, depending on their concentration and nature. The inhibitory effect is generally attributed to blocking steps or poisoning of active sites on the crystalline surface (kinks) [7]. Inhibitor molecules can be adsorbed on all faces of the crystal, reducing the growth rate to zero (nucleation inhibitors) or on specific faces (growth inhibitors), causing a change in the morphology (habit) of the crystals [8].

According to a non classical crystallization approach, nucleation inhibition can be due to the adsorption of the additive on the systems in solution (ion associates or pre-nucleation clusters). This adsorption stabilizes these systems against aggregation and subsequent nucleation[9].

In the case of additives acting as inhibitors, the induction time, that is the period between the establishment of supersaturation and the formation of a new phase at a higher critical supersaturation, increases [10]. Longer induction times and a larger critical supersaturation allow transport of the saline solution to the surface of the porous stone, where crystallization occurs as efflorescence, which is not harmful to the material integrity [3].

When the additives act as promoters, crystallization takes place within the pores at a low supersaturation, and therefore, the crystallization pressure generated is lower [2]. As a consequence, the damage to the substrate in which the salt crystallizes is minimized [3].

While many works focused on the study of the damage caused by crystallization of

sodium [5; 11], calcium [12] and magnesium [6] sulphates, as well as sodium chloride[13], very few studies have dealt with the study of the crystallization mechanisms of sodium carbonates and the stone materials' deterioration processes induced by these salts, although, together with sodium and magnesium sulfates, they are some of the most harmful salts identified in buildings of historical and/or cultural interest [12].

The $Na_2CO_3 \cdot H_2O$ system can be considered an analogue to the case of the $Na_2SO_4 \cdot H_2O$ system, since both have three different phases with equal degree of hydration (monohydrate, decahydrate and heptahydrate, the latter not known in the mineral form [1; 14]), so that their study may be interesting to determine whether the conclusions reached as regards the mechanisms of alteration by crystallization of sodium sulphate salts are general and valid for other hydrated systems. Moreover, it is even expected that the presence of sodium carbonate in historic buildings will increase in the coming years associated with the use of Portland cement (important source of Na_2CO_3 because of its high alkali content) in restoration interventions. These reasons justify the need to perform further studies on the crystallization process of natron ($Na_2CO_3 \cdot 10H_2O$), trona ($Na_3(CO_3)(HCO_3) \cdot 2(H_2O)$), thermonatrite ($Na_2CO_3 \cdot H_2O$), hydrite ($Na_2CO_3 \cdot 7H_2O$) and nahcolite ($NaHCO_3$), being the latter particularly interesting as it is formed at temperatures and pH more similar to the environmental ones than the other crystalline forms [14], and to evaluate the potential use of additives that modify the crystallization process of sodium carbonates (promoting or inhibiting it), with the aim to avoid or minimize the deterioration of porous ornamental rocks caused by these salts.

According to what was stated above, this work aims to determine the best crystallization promoter/inhibitor for sodium carbonate minerals among a series of selected organic additives, in order to avoid/minimize damage due to salt weathering.

To achieve this goal, firstly crystallization test from solution were performed. Once the best modifiers were identified, weathering experiments and pore size analysis were carried out on limestone samples treated and untreated with the best crystallization modifiers found during the first part of the work. At the same time a parallel study (XRD, DLS, calculation of the nucleation density, FESEM) was performed in order to understand what kind of phase precipitated, the sequence of precipitation and the morphology in which these phases precipitate with and without the additives.

Overall, this procedure may give us more details about salt crystallization in natural stones and may help us to gauge the effectiveness of treatments for the prevention of salt damage.

1.1 Salt weathering

Salt weathering is a geomorphic process resulting in the physical disintegration of rocks and stones and in the *fretting* of their surfaces. As reported in several studies, salt weathering is a major hazard for buildings and other engineering structures and this problem has been reported in a wide range of environments [14; 15; 16].

Salt weathering has both physical and chemical components.

Salt-induced physical weathering occurs inside the cracks and pores of a stone material when soluble salts present in water flow through the pore network and undergo cycles of crystallization and dissolution. As water seeps through the network of cracks and pores, it also chemically weathers the stone substrate through dissolution of the stone-forming minerals.

Even if physical and chemical weathering mechanisms occur together and act synergistically to enhance the salt weathering process, physical weathering is by far the more studied aspect of salt weathering.

This process is mainly due to the accumulation of soluble salt in the stone, which crystallize, growth and expand within the porous material [17].

Soluble salts come from a variety of sources including air pollution, bird dropping, microbial activity, marine aerosols and improper use of cement [18; 19; 20]. These salts can also be contained in the same stone structure , as mortars and cements, so in a restoration operation involving the use of a new material to replace or integrate damaged parts of the starting stone structure, it is essential that the material used contains a negligible amount of soluble salts, in order to minimize the formation of undesirable crystalline forms [21].

Soluble salt are mobilized into the stone by water transport. The water dissolves the soluble salts, already present in the surrounding material or environment, and drags them through the pores and capillaries to the external surface of the material and then evaporates. Salts in solutions at the stone surface, as soon as they reach a concentration higher than the saturation one, are able to crystallize forming harmless, but unsightly, *efflorescence* (Figure 1).

Fig.1:a) Salt damage affecting the Baños de Comares at the Alhambra, Granada (Spain). (Photo: E. Sebastian Pardo, [7]), **b)** the Monastery at Petra, Jordan. This heritage site, shows extensive damage due to salt weathering on the bottom part of the structure (Photo: M. Gòmez Heras [7]).

Some studies show that crystal formation strongly depends on the substrate moisture and, in 1989, Zehnder et al. [17] divided the efflorescence growth sequence of sodium nitrate into four phases. The same sequence may be generally extended to others salt systems and is described as follows:

- Step 1: While the surface of the material is still wet, crystals of several hundred microns begin to form (Figure 2a).
- Step 2: The surface is still coated with a thin film of solution within which the previously formed crystal aggregate into clusters of less than 100 μm (Figure 2b).
- Step 3: When the surface is damp, fibrous systems of a few millimeters, consisting of columnar crystals perpendicular to the surface, are formed (Figure 2c).
- Step 4: Sloping or curled whiskers, with a diameter between 10 and 100 μm, in the moderate humid surface, are formed (Figure 2d). They are often polycrystalline and consist of an aggregate of parallel fibers. When the surface is dry the whiskers will thin until reaching a diameter of a few μm (Figure 2e).

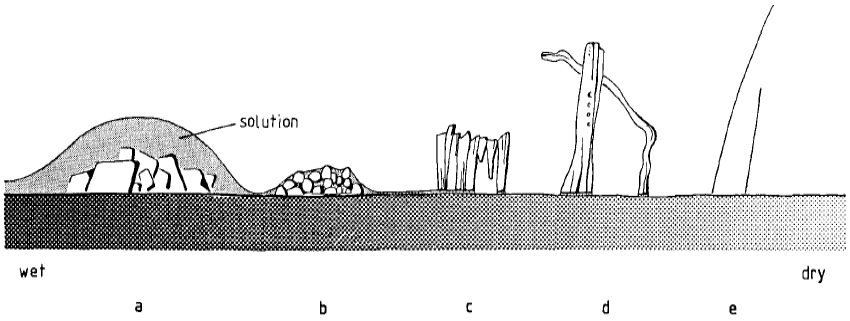

Fig.2: Crystallization sequence of sodium nitrate on a porous substrate [17].

The previously schematized crystallization sequence results to be complete when the relative humidity (RH) is slightly lower than the equilibrium RH of the salt that is crystallizing [17]. The phenomenon is explained by the fact that, within pores with radius smaller than 1μm and contaminated by soluble salts, the chemical-physical effects that determine the equilibrium pressure of the solutions can make the condensation of water to occur at lower RH [22].

When the water evaporation rate is very high, for example during warmer months or in conditions of strong wind, water can't reach the material surface and remains inside them. Thus, the solution reach the supersaturation condition inside the material and salts crystallize in the inner spaces.

These crystalline formations are called *subflorescence* and lead to internal tensions that cause the breakage of the material [22] (Figure 3).

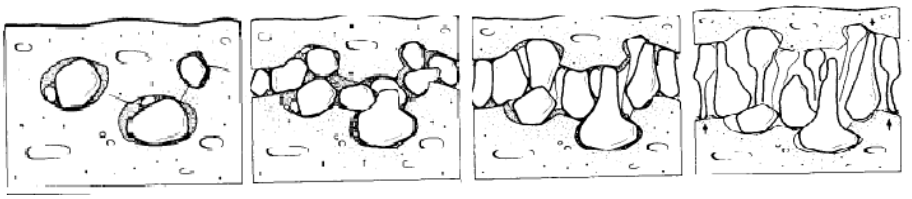

Fig. 3: Crystal growth sequence within a porous material [17].

Responsible for this damage is the crystallization pressure, that is the force applied to the pore walls by the crystallization of salts in a confined space.

So that the crystal growth can continue beyond an initial nucleation, a thin film of liquid (a few nm) needs to be maintained between the crystal and pore wall [1].

It is the repulsive force, not easily measured, between the crystal and the pore wall that ultimately causes the crystallization pressure, rather than a contact force applied by the crystal.

The three kinetic pathways by which high crystallization pressures are most commonly produced are: i) rapid cooling, for salts whose solubility is dependent on temperature, ii) rapid drying, and iii) contact between two solutions, one saturated with respect to one phase and the other one supersaturated with respect to another phase, e.g., thenardite-mirabilite) [23].

Correns in 1949, and many researchers since [1; 22; 23], have found that the crystallization pressure exerted by a crystal growing from a supersaturated solution is proportional to the degree of supersaturation of the solution with respect to the first phase to crystallize out of solution. The equation first published by Correns in 1949 gives crystallization pressure, *P*, as a function of the degree of supersaturation of a saline solution (equation 1):

eq. 1

$$P = \frac{RT}{V_m}\left(ln\frac{C}{C_0}\right)$$

where R is the gas constant, *T* is the absolute temperature, V_m is the molar volume of the crystalline solid, and C/C_0 is the supersaturation ratio (solution concentration over solution saturation concentration).

Alternative versions of this equation have been proposed periodically since then, with some of the latest equations taking into account the geometry of the interface between pore, solution and crystal, as well as the supersaturation at which crystallization occurs [23].

.

1.2 Sodium Carbonate as a weathering agent

Different soluble salts can be responsible for the type of physical weathering previously described, like sodium sulphate[5; 11; 23; 24], without doubt one of the most studied, magnesium sulphate[6], calcium sulphate[12] and sodium carbonate[25].

Despite that very few studies have investigated the crystallization mechanisms of sodium carbonates and the processes of stone materials deterioration induced by these salts, they represent some of the most harmful salts identified in buildings of historical and/or cultural interest, as shown in table 1 [14].

Pedro (1957)	Kwaad (1970)	Goudie et al (1970)	Goudie (1974)	Goudie (1974)	Goudie (1986)	Goudie (1993)[a]	Goudie (1993)[b]
$NaNO_3$	Na_2SO_4	Na_2SO_4	Na_2SO_4	Na_2SO_4	Na_2CO_3	$NaNO_3$	Na_2SO_4
Na_2SO_4	Na_2CO_3	$MgSO_4$	$MgSO_4$	Na_2CO_3	$MgSO_4$	Na_2CO_3	Na_2CO_3
$Mg(NO_3)_2$	$MgSO_4$	$CaCl_2$	$CaCl_2$	$NaNO_3$	Na_2SO_4		$NaNO_3$
K_2SO_4	NaCl	Na_2C0_3	Na_2CO_3	$CaCl_2$	NaCl		$MgSO_4$
KNO_3	$CaSO_4$	NaCl	$NaNO_3$	$MgSO_4$	$NaNO_3$		NaCl
Na_2CO_3				NaCl	$CaSO_4$		
K_2CO_3							
$MgSO_4$							
$CaSO_4$							
$Ca(NO_3)_2$							

Tab. 1: The relative effectiveness of different salts in salt weathering experiments ranked from high to low [12]. [a] Results obtained with Wadi Digla Cycle; [b] Results obtained with Negev Cycle [14].

Sodium carbonate crystalline forms are different and differ in their degree of hydration.

The $Na_2CO_3{\cdot}H_2O$ system is similar to the $Na_2SO_4{\cdot}H_2O$ system: it presents two stables mineral phases (natron, $Na_2CO_3{\cdot}10H_2O$, and thermonatrite, $Na_2CO_3{\cdot}H_2O$) and a metastable heptahydrate phase (hydrite, $Na_2CO_3{\cdot}7H_2O$) not known in the mineral form.

In addition, two other hydrous sodium carbonate minerals are known and commonly formed in nature: trona ($Na_3(CO_3)(HCO_3){\cdot}2(H2O)$) and nahcolite ($NaHCO_3$) [15] (Figure 4). Others crystalline forms, like wegscheiderite ($Na_2CO_3{\cdot}3NaHCO_3$) [26], are very rare and can be omitted in this discussion.

a)

Nahcolite Trona Natron Thermonatrite

b)

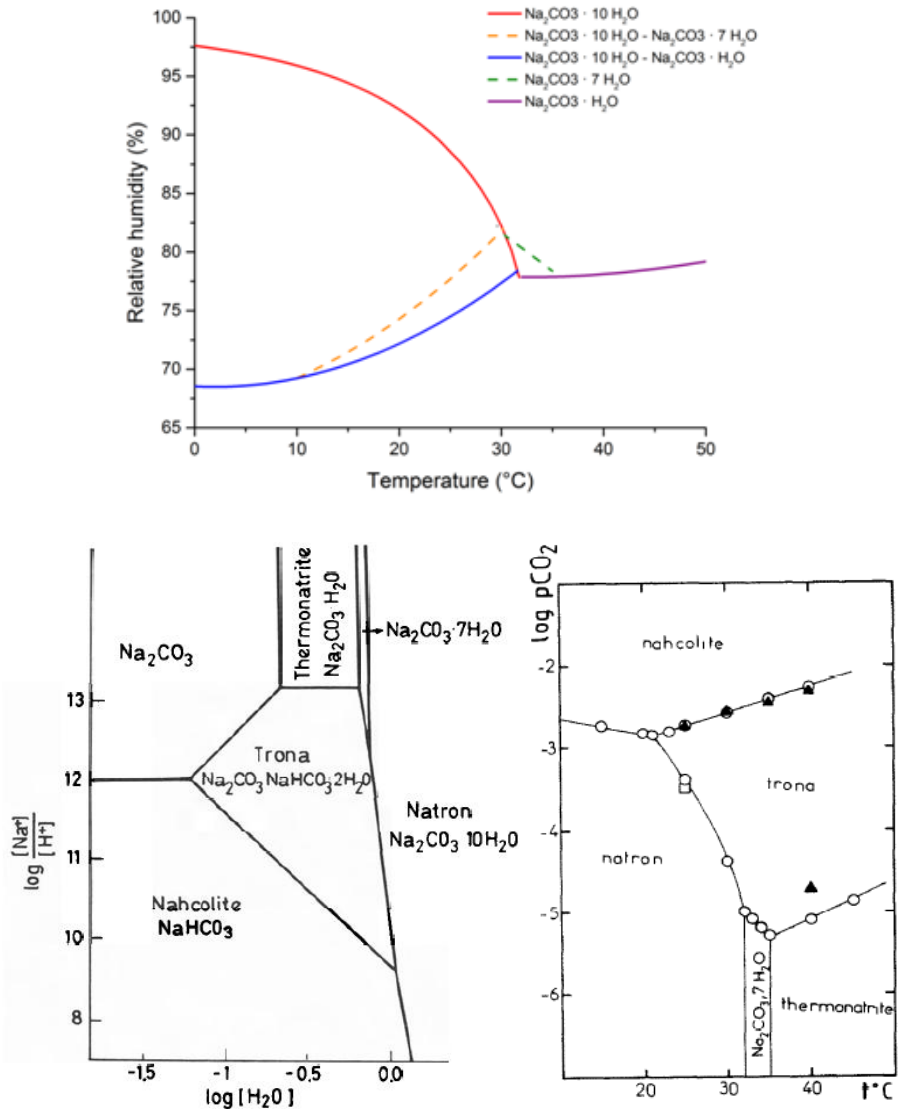

Fig.4: Main Sodium Carbonate crystalline forms. a) Photos of nahcolite, trona, natron and thermonatrite in mineral form[27] . b) Phase diagrams for the system of Na_2CO_3 and water in: relative humidity vs. temperature [28]; log [Na+]/[H^+] vs. log [H_2O] [16]; log(pCO_2) vs. temperature [29].

As shown in Figure 4b, sodium carbonate hydrate phases are formed at different relative humidity, pH and temperatures. For many years it was believed that the formation of a

hydrated phase leads to an increase in volume of salt and thus develops pressure against pore walls [30].

However several workers have shown that damage due to crystallization pressure appears to be more important than damage due to hydration pressure [2; 31; 32]. For example, for sodium sulphate it was demonstrated that the generation of pressure is due to the dissolution of the lower hydrate phase (thenardite, Na_2SO_4) and the subsequent precipitation of the higher hydrate (mirabilite, $Na_2SO_4 \cdot 10H_2O$) at high supersaturation [2; 33].

Regarding sodium carbonate, there are not many studies in the literature about the effect of crystallization pressure. Benavente et al. [15], have studied the crystallization pressure that result from changes in temperature of the most common and aggressive salts that generate stress in porous building. The results show that the variation of crystallization pressure with temperature for the transition thermonatrite ($Na_2CO_3 \cdot H_2O$) - natron ($Na_2CO_3 \cdot 10H_2O$) is equal to 0.9 MPa/°C, a high enough value to explain the aggressive character of these salts.

Major studies have been carried out on the hydration of sodium carbonate [14].

It has been seen that the percentage volume change from the anhydrous form (Na_2CO_3) to decahydrate form ($Na_2CO_3 \cdot 10H_2O$) is 374.7% and that sodium carbonate absorbed about half as much humidity of magnesium sulphate [14] (Figure 5).

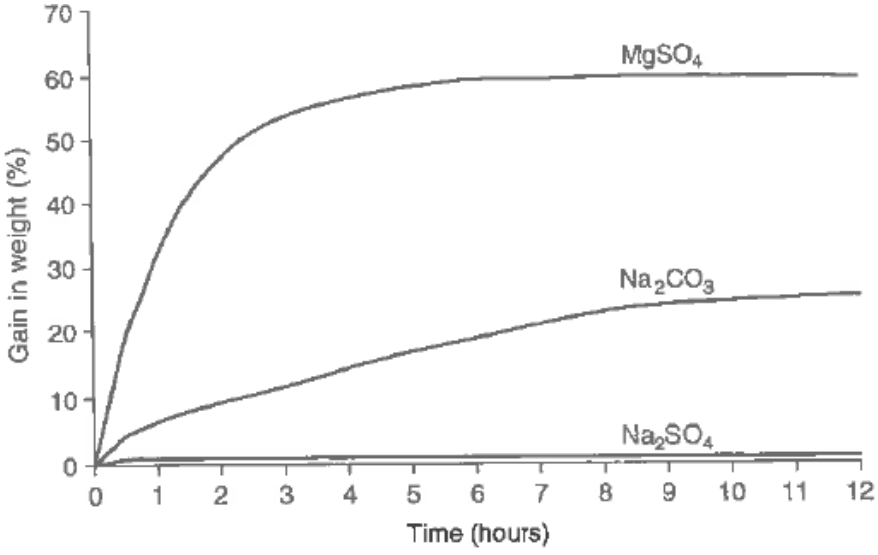

Fig. 5: Hydration rate of MgSO4, Na2CO3 and Na2SO4 at 20°C and at relative humidity of 90%. Salts were dried to a constant weight at 105°C before the experiment [14].

Moreover, Winkler and Wihelm in 1970 [30] calculated hydration pressure (table 2) values for thermonatrite ($Na_2CO_3 \cdot H_2O$) to hydrite ($Na_2CO_3 \cdot 7H_2O$) and hydrite ($Na_2CO_3 \cdot 7H_2O$) to natron ($Na_2CO_3 \cdot 10H_2O$).

a. $Na_2CO_3 \cdot H_2O \rightarrow Na_2CO_3 \cdot 7H_2O$

Hydration pressure [atm]

		Temperature [°C]			
		0	**10**	**20**	**30**
Relative Humidity [%]	**100**	938	770	611	430
	90	799	620	457	276
	80	637	455	284	94
	70	448	264	88	-
	60	243	46	-	-

b. $Na_2CO_3 \cdot 7H_2O \rightarrow Na_2CO_3 \cdot 10H_2O$

Hydration pressure [atm]

		Temperature [°C]			
		0	**10**	**20**	**30**
Relative Humidity [%]	**100**	816	669	522	355
	90	666	504	350	185
	80	490	320	160	0
	70	282	112	0	-
	60	60	-	-	-

Tab.2: Hydratation pressure of (a) thermonatrite ($Na_2CO_3 \cdot H_2O$) to hydrite ($Na_2CO_3 \cdot 7H_2O$) and (b) hydrite ($Na_2CO_3 \cdot 7H_2O$) to natron ($Na_2CO_3 \cdot 10H_2O$) versus temperature and relative humidity [30]

To calculate the hydration pressures listed in table 2, we can follow the equation proposed by Mortensen in 1933[34] (equation 2):

eq. 2

$$P = \frac{RT}{V_m} \ln\left(\frac{P_1}{P_2}\right)$$

where P is the hydration pressure, T is the absolute temperature, V_m the molar volume of water of crystallization, R the gas constant, P_1 the vapor pressure of water at the temperature T and P_2 the dissociation pressure of the hydrated form at T.

Since then, a number of variations were proposed for the calculation of hydration pressure [30].

Despite the previous studies made on sodium carbonate, as for the sodium sulphates, the so-called "hydration pressure" is discredited as a plausible mechanism for salt damage in salt systems with various hydrated phases like sodium carbonate. Therefore, much research is needed to figure out how damage occurs due to the crystallization of the different salts than can form in the $Na_2CO_3 \cdot H_2O$ system.

1.3 Crystallization from solution

Considering that crystallization inhibitors/promoters act on the crystallization process of a salt, the key aspects of the nucleation process and crystal growth theory need to be taken into account to better understand the effect of these additives.

The formation of crystals in solution takes place in two steps. Firstly, nucleation takes place. The nucleation step corresponds to the production of clusters of ions or molecules from which spontaneous growth may subsequently occur. Secondly, the growth of these nuclei through the incorporation of various growth units [35].

Nucleation can be homogeneous, if the origin of the new phase is not influenced by the presence of a pre-existing solid phase (or interface), or, conversely, heterogeneous.

In this work we will always talk about homogeneous nucleation.

The nucleation of a crystal from solution depends on three main factors: the supersaturation (σ) of the solution, the crystal-solution interfacial energy (γ), and the molecular volume (Ω) of a critical nucleus [36].

Supersaturation is a measure of how far the system is from equilibrium conditions when crystallization begins. It can be obtained either by cooling, or more generally, by evaporation. There are several ways to express supersaturation, however the most common ones are the following ratios: IAP/Kps, where IAP is the Ion Activity Product and Kps the solubility constant [37]; a/a_0, where a is the activity of the dissolved ions in the supersaturated solution and a_0 is the activity of the saturated solution [38]; and C/C_0, where C is the solution molar concentration and C_0 is the solution saturation molar concentration [37].

Interfacial energy is the work required to build an area of a particular surface. Phases with very low values of interfacial energy are more soluble and do not tend to reach a high supersaturation during crystallization. Conversely, salts with a high interfacial energy, typically less soluble, do tend to achieve a high supersaturation [39].

Once a sufficiently high concentration of salts in solution is achieved, nucleation of a solid phase, called *nucleation cluster*, occurs.

The Classical Nucleation Theory (CNT), originated with the works of Gibbs in the late 1800 [40; 41], indicates that the driving force for nucleation is the reduction in overall Gibbs free energy of a system, ΔG, which can be expressed as (equation 3):

eq.3

$$\Delta G = \frac{-4/3\ \pi r^3}{\Omega} kTln(\sigma) + 4\pi r^2 \gamma$$

where r is the radius of the nucleation cluster (assumed to be spherical according to Gibbs[40]), Ω is the molar volume divided by Avogadro's number, k is the Boltzmann constant, σ is the supersaturation, and γ is the surface energy of the nucleation cluster in contact with the solution.

The first term in equation (3) is a bulk term that expresses the fact that the solid is more stable than the supersaturated fluid. In others words, it quantifies the reduction in chemical potential achieved by the formation of a bulk solid phase resulting in energy release. Because of that, this term is negative and proportional to the volume of the crystallite. The second term is a surface term that takes into account the free energy cost of creating a solid–liquid interface. This term is positive and proportional to the surface area of the crystallite [37] (Figure 6).

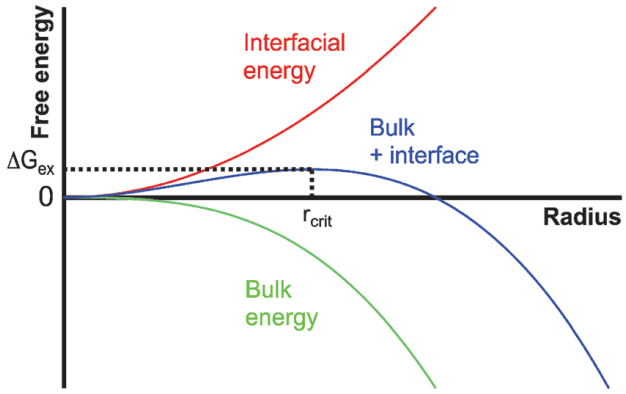

Fig.6: Schematic illustration of the size dependence of the energetics of nanoscopic nuclei within the framework of classical nucleation theory. For a critical cluster radius, r_{crit}, the value of ΔG reaches a maximum (ΔGex) and for $r > r_{crit}$ it decreases [42].

As shown in Figure 6, the sum of the two terms in equation (3) has a maximum that occurs when $d\Delta G/dr = 0$.

This maximum value, ΔG_{ex}, corresponds to the critical nucleus, r_{crit}, and for a spherical cluster is obtained by maximizing equation (4):

eq. 4

$$r_{crit} = \frac{2\Omega\gamma}{kTln(\sigma)}$$

Combining equations (3) and (4) the critical over-all excess free energy for nucleation is given by equation (5):

eq. 5

$$\Delta G_{ex} = \frac{16\pi\Omega^2\gamma^3}{3[kTln(\sigma)]^2}$$

The existence of such a free energy barrier for nucleation is responsible for the system needing to be supersaturated before nucleation starts. Moreover this shows that the behavior of a newly created crystal nucleus in a supersaturated solution depends on its size; it can either grow or redissolve. Hence, the critical radius, r_{crit}, represents the minimum size of a stable nucleus. If the particle is smaller than it will dissolve because only in this way can it achieve a reduction in its free energy. Likewise, if a particle is larger than r_{crit} it will continue to grow.

Based on the above considerations, through equation (6) it is possible to predict the nucleation density, which represent the frequency with which atoms successfully transfer from the parent phase into the nucleus, for any material at a given level of supersaturation [43]:

eq. 6

$$I^b = \frac{kT}{\pi\Omega^{5/3}\eta} exp\left(\frac{-r\Delta\mu + 4r^{2/3}\cdot\gamma}{\mathrm{kT}} f(\theta)\right)$$

where η is the solution viscosity, θ is the contact angle between crystal and substrate, which for homogenous nucleation is assumed equal to 1 (Espinosa-Marzal R.M, personal communication) and Δμ is the difference between the chemical potentials of ions in solution and nuclei, which is directly related to the supersaturation.

However, values calculated can differ by orders of magnitude from experimentally measured data for two main reasons [42].

First of all, the actual surface energy values of crystals at the relevant sizes for nucleation are largely unknown, so that they are assumed to correspond to those of bulk crystals. This assumption is called capillary approximation [42].

Secondly, according to classical nucleation theory, nucleation clusters are assumed spherical [40; 41]. Thus CNT shows a limited ability to describe the behavior of real systems in many cases.

As soon as stable nuclei, particles larger than the critical size, have been formed in a supersatured solution, they begin to grow into crystals of visible size.
The growth of a crystal from a solution takes place in 4 steps [44; 45]: i) the diffusion of ions in solution at the interface solution-crystal onto which they will be adsorbed (Figure 7a), ii) through 2D surface diffusion they are attracted to an energetically favorable site (*step*) (Figure 7b), iii) monodimensional diffusion along the step up to a *kink* (Figure 7c), iv) Incorporation of crystal constitutional units into the lattice (Figure 7d).

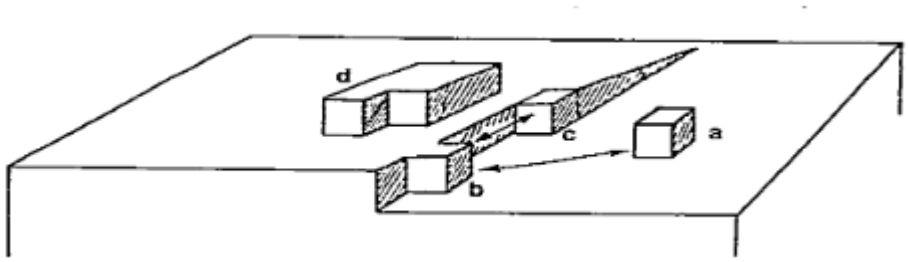

Fig. 7: Representation of a crystal surface showing the development of an emerging growth step[44].

In view of the above, crystals of variable dimensions will be found in solution. Larger crystals continue to grow at the expense of the smallest through a maturation process called "Ostwald's ripening". The mechanism is driven by thermodynamic stability, so larger particles are energetically favored compared to smaller particles due to the higher superficial surface tension that characterizes the latter. In fact, the molecules on the surface of the particles are energetically less stable than the inside ones. Because of that smaller particles, which have a higher surface/volume ratio than large particles, also have higher surface tension and therefore will be more reactive. In solution, smaller particles will therefore tend to solubilize by increasing the concentration of free molecules in solution. When the concentration of free molecules becomes supersaturated, they tend to deposit on the surface of the larger particles. Therefore, all smaller molecules will tend to disintegrate by favoring the growth of large ones, thus decreasing the overall surface energy of a system [35].

Despite the successful application of CNT and classical crystal growth theory over the last 100 years, recent experimental and computational studies are showing that in several natural, laboratory, and industrial systems, crystallization strongly deviates from the classical picture [46]. However, little is known about the applicability and importance of these non-classical crystallization mechanisms in the case of the salt system studied here so, in the rest of this work, we will mention the key points of non-classical crystallization to understand the influence of additives, while the thermodynamic treatment of crystallization will follow the CNT.

1.4 Crystallization modifiers

Inhibition of salt crystallization by additives has been known for a long time and has gained great interest in various industrial processes: prevention of valve and pipes clogging for the passage of gas and oil [47; 48], industrial boilers, heat exchangers, water pipes, desalination plants [49].

Additives were also used to delay crystallization in cements [50] and gypsum plasters [51].

Additives strongly influence the main stages of crystallization and crystalline maturation. The consequences of this may be one or more of the following: impossibility of nucleation, change in the number and size of the crystals, modification of the morphology or the type of precipitated phase [37].

As already stated there are two class of inhibitors: nucleation inhibitors and growth inhibitors.

According to Gebauer et al. [9], nucleation inhibitors act in the prenucleation stage and they can be categorized in two main types:

- type I: acting through adsorption of cations;
- type II: acting through adsorption on prenucleation clusters and their stabilization.

The additives used to inhibit crystallization are mostly organic molecules that possess one or more functional groups. Such functional groups, at appropriate pH conditions [5], can establish electrostatic interactions or hydrogen bonds with systems in solution (ions, pre-nucleation clusters, nucleation embryos, or organic molecules, the latter of particular interest in the pharmaceutical industry [52; 53]) [5; 53].

As an example of this kind of interaction, in Figure 8 it is shown how cations in solution are bound by citric acid [51].

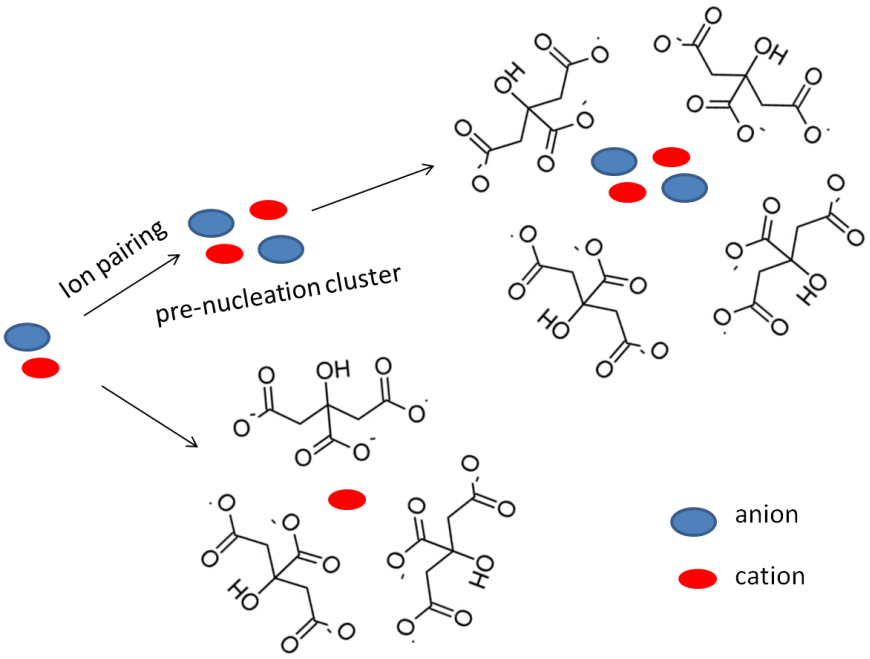

Fig. 8: Interaction between citric acid and cations in solution.

As seen in Figure 8, additives can act in the pre-nucleation stage by adsorption of ions and clusters. This adsorption stabilizes the system against nucleation, that is, against aggregation of ions and clusters.

For nucleation to occur, this inhibitor–ion/cluster interaction has to be broken so that ions/clusters can diffuse in solution and form a critical nucleus.

Therefore, based on the strength of these interactions, nucleation can be delayed/ inhibited [53].

As for growth inhibitors, their effect is to reduce the incorporation rate of crystal constitutional units within the lattice. [8]

They act by adsorption on specific crystal sites, in particular three sites may be considered at which inhibitor species may become adsorbed and hence reduce the layer formation velocity: at a kink (Figure 9a), at a step (Figure 9b) or on a ledge between steps (Figure 9c) [54].

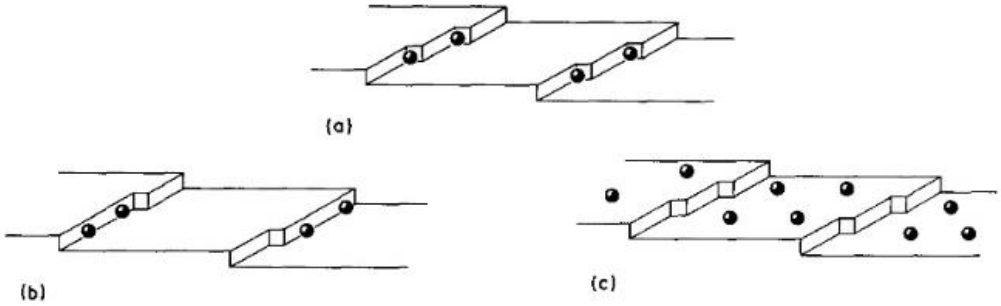

Fig. 9: Sites for impurity adsorption on a crystal surface [54]

Adsorption at *kinks* would effectively reduce their number and, since they are the sites at which growth units are incorporated into the lattice, reduce the layer formation velocity.
Further, an increase in the *interkink* distance would reduce the importance of surface diffusion in the growth process. As pointed out by Bennema [55] and Larson [57], this would lead to a situation in which the rate of advance of the steps would depend on the density of *kinks* and would result in polygonisation of the growth layers.
Adsorption of impurities giving monolayer coverage at a step would reduce the number of sites available for growth at the step and hence would reduce its velocity.
However, for adsorption of impurities corresponding to less than monostep coverage, the advancing step could squeeze between the inhibitor species relatively not unimpeded. This mechanism thus implies a critical concentration of inhibitors in solution, below which the layer formation velocity would be unaffected and above which it would rapidly decrease [58].
Adsorption of inhibitors on a ledge is applicable in cases where the surface processes, particularly surface diffusion, play an important role in the growth process [59].
The result would be to decrease the surface area and the surface flux of growth units to the step, thus reducing the layer formation velocity.

Certain additives can also act as crystallization promoters. The term promotion is often invoked to describe a wide range of phenomena, which include the modification of crystal size or number of nuclei, the rate or degree of intercrystalline aggregation, and the adsorption or epitaxial growth of crystals at interfaces [60]. Here, we specifically refer to promotion as the ability of a modifier to accelerate the kinetics of nucleation and/or crystal growth.
As already stated in section 1.3, in the homogenous nucleation process, a nucleation embryo must overcome a free-energy nucleation barrier before it can reach a critical radius, and become a stable growing crystal.
In the presence of some additives or other foreign objects (e.g., organic substrates for biomineralization processes [61]), the nucleation barrier is reduced to :

eq. 7

$$\Delta G = \Delta G_{homo} f(m, x)$$

where f(m, x) is the interfacial correlation factor, varying from 0 to 1, describing the lowering of the nucleation barrier due to the presence of additive molecule or the substrate.

This factor will depend on supersaturation, the interfacial interaction parameter *m* and the relative size of foreign particles *x*.

The interfacial interaction parameter and the size of foreign particles can be expressed by the following equations (equation 8; equation 9) :

eq. 8

$$m = \frac{(\gamma_{af} - \gamma_{ac})}{\gamma_{cf}}$$

eq. 9

$$x = \frac{R_s}{r_{crit}}$$

where γ_{af} and γ_{ac} are the interfacial free energies of the foreign particle (a)-fluid (f) interface and of foreign particle-crystal nucleus (c) interface respectively; γ_{cf} is the interfacial free energy between the crystal nucleus and the fluid, depending on the correlation and structural match between the nucleating phase and the substrate; R_s is the average radius of spherical shaped foreign particles [62].

When the interaction between the nucleating phase and the foreign substance is optimal, f(m, x) → 0. Conversely, if the interfacial correlation is very poor, f(m, x) → 1, and the additive molecule exerts almost no influence on the nucleation barrier.

As the critical radius depends on the supersaturation (see section 1.3, equation 4), the interfacial interaction parameters, f(m, x), will increase with supersaturation [62].

This implies that an increase of supersaturation will drive the crystal from an interfacial structural match state (a lower f(m, x)) to a state of higher mismatch (a higher f(m, x)).

It follows that a good structural synergy between crystal and additive molecules will promote an ordered crystal structure and occurs only at low supersaturations [62].

In view of the above, during a restoration/conservation intervention, it is essential to provide for the use of inhibitory/promoter substances in order to avoid/minimize stone material damage. The object of this work is therefore the search for organic substances

capable of inhibiting/promoting the formation of sodium carbonate hydrate forms and the analysis of their action on the crystallization process.

2. Materials and methods

2.1 Salt solution and crystallization modifiers

For crystallization experiments, $NaHCO_3$ solutions (12% w/w, pH 7.9) were prepared from anhydrous solid (Sigma Aldrich; purity 99.7-100%) and deionized MilliQ water (MilliQ filtration system, Millipore Corporation, pH 5.96, resistivity >18.2 MΩ) to which different amounts of the tested additives were added to give final concentrations of 0.1, 1 and 10 mM.

The additives chosen for crystallization test were (Figure 10): sodium citrate tribasic dihydrate (CA), L-aspartic acid sodium salt monohydrate (AAS), polyacrylic acid 2100MW (PA), etidronic acid (HEDP), aminotris(methylenephosphonic) acid (ATMP) and diethylenetriaminepentakis-(methylphosphonic) acid (DTPMP).

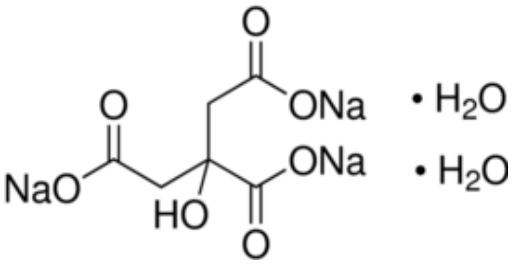

a) Sodium citrate tribasic dihydrate (CA)

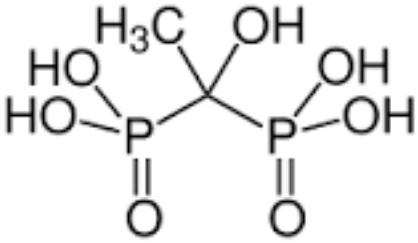

d) etidronic acid (HEDP)

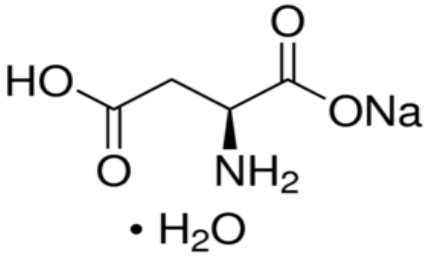

b) L- aspartic acid sodium salt monohydrate (AAS)

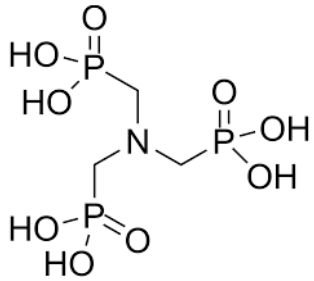

e) aminotris(methylenephosphonic) acid (ATMP)

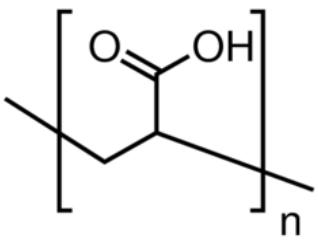

c) polyacrylic acid 2100MW (PA)

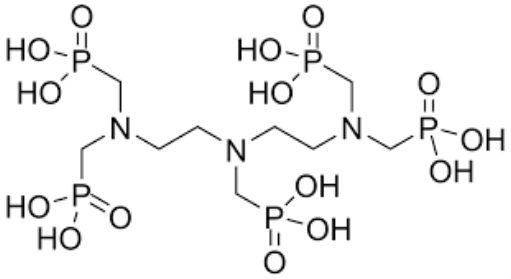

f) diethylenetriaminepentakis-(methylphosphonic) acid (DTPMP)

Fig. 10: Molecular structure of **a)** CA, **b)** AAS, **c)** PA, **d)** HEDP, **e)** ATMP, **f)** DTPMP.

From now on, during the discussion only the abbreviations will be used to indicate these substances.

In table 3 their molecular weight, chemical formula, manufacturer and purity are indicated.

Additive	Molecular weight [g/mol]	Chemical formula	Manufacturer	Purity
CA	294.10	$C_6H_5Na_3O_7 \cdot 2H_2O$	Sigma Aldrich	99%
AAS	173.11	$C_4H_6NNaO_4 \cdot H_2O$	Fluka	≥99.0%
PA	2100	$(C_3H_4O_2)_n$	Fluka	≥97.0%
HEDP	206.03	$C_2H_8O_7P_2$	Sigma Aldrich	≥95%
ATMP	299.05	$C_3H_{12}NO_9P_3$	Sigma Aldrich	≥97.0%
DTPMP	573.20	$C_9H_{28}N_3O_{15}P_5$	Sigma Aldrich	liquid

Tab.3: Molecular weight, chemical formula, manufacturer and purity of the additives used.

These additives where selected because they are commonly used as crystallization modifiers in industrial [63] and medical [54] applications or for desalination and water treatment [64].

Phosphonic acid derivatives (phosphonates) are the most well-known and most industrially used[65]. They can increase by several hundred times the level of supersaturation of sparingly soluble calcium salts [65; 66; 67], are thermodynamically stable compounds and do not hydrolyze in water at any pH, even at high temperatures. At concentrations equal to and above the stoichiometric, and depending on the pH, they are effective metal ion sequesters [67]. Moreover, depending on the crystalline phase, they act as inhibitors even if used in trace amounts [68].

Polyelectrolytes, together with phosphonates, are the most widely used inhibitors. The most common are polyacrylates, polymethacrylates, polyacrylamides, polymaleates and their copolymers. They have good thermal and hydrolytic stability [63].

Polycarboxylic acids or their polymeric analogs and derivatives have been successfully used as crystallization inhibitors of calcite, fluorite and gypsum [69;70].

The main advantage of some of them is that they do not contain phosphorus or nitrogen, so their use as crystalline phase inhibitors does not imply the introduction of nutrients for microorganisms that would cause water quality problem[69; 71].

2.2 Salt crystallization test from solution

In order to identify which of the substances reported in section 2.1 works as an inhibitor/promoter, increasing/lowering the critical supersaturation of the solution made with sodium bicarbonate, bulk crystallization experiments were performed.

100 ml of sodium bicarbonate solution, prepared as explained in section 2.1, were placed in a jacketed reactor, which was closed and connected to a water bath for the control of the internal temperature, and magnetically stirred at a moderate speed. The system temperature was slowly lowered from 55 to 2°C. These temperatures were chosen because 55°C corresponds to the equilibrium *T* (the temperature at which the free energy of the liquid is equal to the free energy of the crystal) of a solution 12% w/w of $NaHCO_3$[71] and 2°C is a temperature which allows not to cool too much the water in the water bath while reaching as sufficiently high undercooling (i.e., supersaturation) as to enable crystallization.

During slow cooling (0.6°C/min), temperature, conductivity, transmittance and pH of solutions were monitored starting from 35°C using Metrohm probes.

As the nucleation consists in the initial appearance of a new phase during a first- order phase transition, the crystallization onset can be detected visually (Figure 12) using the Metrohm Optrod, a sensor for transmittance. This probe can work with eight different wavelengths for a wide measuring range. In this study the wavelength selected was 610 nm.

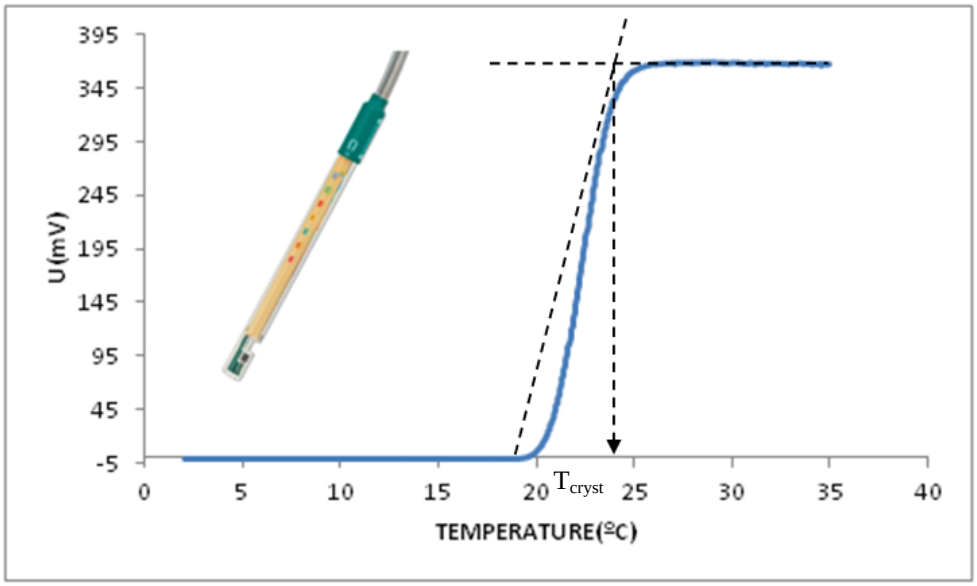

Fig. 12: Curve obtained through Metrohm Optrod during the slow cooling of the system (solution containing ATMP 1 mM). The crystallization temperature is obtained as shown by the black dashed lines.

As shown in Figure 12, the portions of the curve both prior to and after the inflection point are reasonably linear, then the intersection of tangents to these lines will accurately locate the inflection point. The temperature corresponding to the intercepted point is the crystallization Temperature (T_{cryst}).

According to Marti et al. [71], the visual detection of salt crystallization Temperature results in comparable accuracy with that of other techniques, like conductivity measurements. Moreover, visual detection of salt crystallization onset was highly reproducible, as will be showed in "*Results and Discussion*" (see section 3.1).

After reaching a temperature of 2°C, stirring and cooling were stopped and solutions were filtered under vacuum through millipore filters of cellulose nitrate (Ø < 0.4μm) and the precipitate, when formed, was analyzed using x-ray diffraction (see section 2.3).

Experiments were repeated in triplicate.

The thermodynamic code PHREEQC was used to calculate the saturation index (Ω=IAP/Kps) for the experimentally determined crystallization temperature.

The Pitzer database was used for such calculations [15].

Regarding the dependence of the solubility products of sodium carbonate crystalline forms with temperature, PHREEQC uses the Van't Hoff equation (equation 10), with the adjustment parameters given by Monnin and Schott (1984) [29]:

$$\log Kps = A_1 + A_2 \cdot T + A_3/T + A_4 \log T + A_5/T^2 \qquad \text{eq. 10}$$

Where *T* is the temperature in Kelvin and A_i are fitting parameters [15], that according to Monnin and Scott [29] for crystalline forms of sodium carbonate assume the values listed in table 4.

Crystalline form	**Formula**	**A_1**	**A_3 [K]**
Nahcolite	$NaHCO_3$	7.7±0.7	-2570±200
Natron	$Na_2CO_3 \cdot 10H_2O$	28.3±0.3	-9000±85
Trona	$Na_3(CO_3)(HCO_3) \cdot 2(H2O)$	10.5±2.1	-3800±630
Thermonatrite	$Na_2CO_3 \cdot H_2O$	0.05±1.41	360±420
Hydrite	$Na_2CO_3 \cdot 7H_2O$	19.9±0.5	-6230±150

Tab. 4: Fitted parameter for sodium carbonate crystalline forms [29]. The fitted parameters of equation 10 not listed in this table are equal to zero.

In this way, these experiments will allow evaluation of the effectiveness of the tested additives as inhibitors or promoters, by comparison with the supersaturation reached in the absence of additives. From these results the most effective additives and their concentration will be selected to be used in crystallization experiments within porous materials (see section 2.5).

2.3 X-ray diffraction (XRD) investigations

Crystalline materials are characterized by interatomic distances of the same order of magnitude of the X-ray wavelengths, so they can produce their diffraction.

This phenomenon is the basis for X-ray diffraction analysis: through the diffraction angle measurements, crystalline materials can be identified.

The X-ray diffraction conditions can be described by considering the diffraction of a monochromatic beam on a row (plane) of atoms or ions (Figure 13)[73].

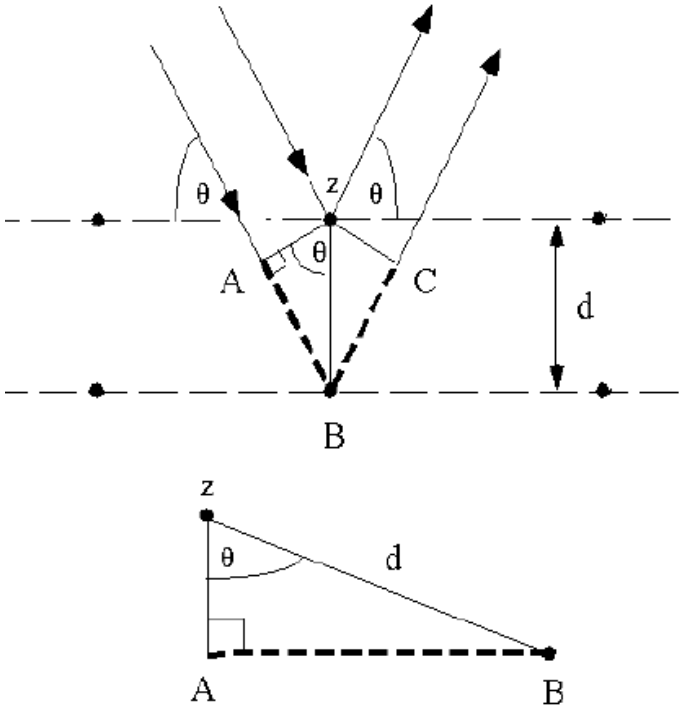

Fig. 13: Light interaction with atoms of crystalline planes. Graphic representation of Bragg's law [73].

From the graphic representation shown in Figure 13, Bragg's law is deductible (equation 11):

$$n\lambda = 2d \sin\theta \qquad \text{eq. 11}$$

Where *n* denotes the order of diffraction, θ the angle that the incident beam forms with the crystalline plane; λ the wavelength of the radiation and *d* the distance between two adjacent planes.

Diffraction can be considered as the sum of coherent interference phenomena; if a source emits a ray that invests the sample, the ray may be "reflected" both from the surface and

from the reticular plane below. These two rays have the same wavelength, because they are monocromatic, but they can give rise to interference, because they are travelling different distances.
So, the diffused radiation that is out of phase will interfere in a destructive mode and will not be observable, while constructive interference will differ from zero.
From Bragg's Law, if λ is known, one can derive the value of *d* for each of sen θ value which corresponds to an intensity different from the background noise.
The distance between the crystalline planes gives information on the reticular geometry, while the intensity of peaks provide information about the spatial arrangement of atoms in the cell.
Since each phase has a characteristic disposition of atoms, x-ray diffraction can be used to identify the phases [74].

In this work, analysis of the solid collected after crystallization tests from solution were performed whit a Pananalytical XPert Pro, in order to identify and quantify the precipitated phases.
This instrument is equipped with a Copper X-ray source (CuK_α radiation λ= 1.5405 Å) and collects data with working conditions of 45kV, 40 mA, scan field 5º to 70º at a counting rate of 2s / º2θ, scan time of 10 minutes and sample holder rotation of 0.004 r.p.m.
Experimental conditions in the laboratory were as follows: 23°C, RH 39.8%.
Samples were prepared by placing a little amount of solid with a spatula on a sample holder equipped with an aluminum support.
It has to be specified that samples were analyzed immediately after filtration in order to maintain as much as possible the original hydration degree and not inducing the formation of dehydrated phases.

Once selected the best crystallization modifiers (see section 3.1), with the same equipment and experimental conditions, XRD analysis of phases formed following evaporation of the sodium bicarbonate solutions (with and without additives) were performed. These so-called "evaporation tests" were performed according to the following experimental protocol:
A 100 μL drop of saturated $NaHCO_3$ solution with and without additives was placed on a zero background XRD sample holder made of a silicon crystal.

The work conditions during XRD analysis were the same utilized after the crystallization tests from the solution above described, except for the scanning time and the scan field (2° to 60°).

Successive scans were collected continuously throughout the evaporation of the solution until complete crystallization. In total, ten patterns for each solution were collected. The first nine patterns were collected at a scan time of 7 minutes while the scan time of the last pattern was 55 minutes.

This method does not provide a very precise timing of formation since there will be no sign that a new phase has crystallized until enough crystals of that phase have formed to present peaks discernible from the background noise.

However, these analyses allowed us to make some observations about the order in which the phases are formed.

2.4 Dynamic light scattering (DLS) investigations

Dynamic Light Scattering (DLS), also known as Photon Correlation Spectroscopy or Quasi-Elastic Light Scattering, is one of the most popular light scattering techniques because it allows particle sizing down to 1 nm diameter.

Typical applications are emulsions, micelles, polymers, proteins, nanoparticles or colloids.

The basic principle is simple: the sample is illuminated by a laser beam and the fluctuations of the scattered light are detected at a known scattering angle θ by a fast photon detector (Figure 14).

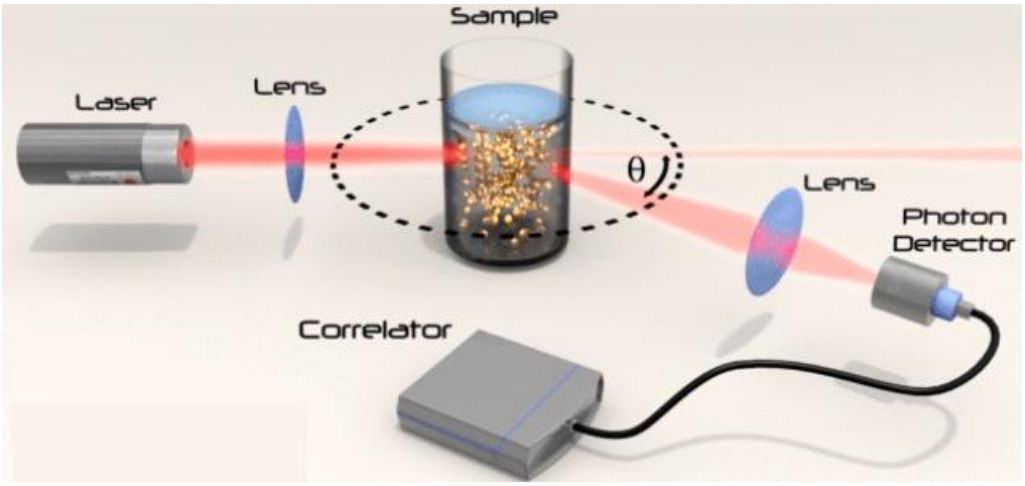

Fig. 14: Schematic illustration of DLS apparatus [75].

From a microscopic point of view, when the light hits small particles, the light scatters in all directions (Rayleigh scattering). Even if the light source is a laser, and thus monochromatic and coherent, the scattering intensity fluctuates over time.

Fluctuations are generated by Brownian particle motions. At the same temperature and viscosity, the smaller particles move quickly, creating rapid changes in the scattering intensity, while the larger particles move slower, resulting in slow intensity variations. Thanks to a correlator, the velocity of intensity variations is measured and the particle diffusion coefficient (D) calculated from the correlation function.

Through the Stokes equation (equation 12) it is then possible to convert the diffusion coefficient into hydrodynamic diameter, assuming the particles are spherical [76]:

$$D = \frac{k_b T}{6\pi\eta d_h} \qquad \text{eq. 12}$$

where D is the diffusion coefficient, k_b the Boltzmann constant, T the absolute temperature, η the viscosity of the system and d_h the hydrodynamic diameter of the particles.

The hydrodynamic diameter refers to the diameter of the particle in its environment and therefore strongly depends on the surrounding area.

As regards to not spherical particles, rotational motion must be considered as well because the scattering of the light will be different depending on orientation.

For a non spherical particle, DLS will give the diameter of a sphere that has the same average translational diffusion coefficient as the particle being measured.

In this work, analysis of crystal growth in solution with and without additives was performed during crystallization tests from solution through a Nanotrac Flex, 180° DLS (Microtrac), in order to analyze the effect of the selected additives during the nucleation and growth of sodium (bi)carbonate crystals.

This DLS is equipped with an external flexible probe that allows to perform in-situ particle size analysis during the progress of all the crystallization tests. An optical fiber located inside the flexible probe allows to direct the laser light to the particles and to return the reflected and scattered light to the detector (Figure 15). This method is called "reference beating" and is an accurate method to measure particle size distribution of nanoparticles. The reflected light intensity, in fact, is superior to the scattered one, so the resulting signal is stronger than the noise contribution [77].

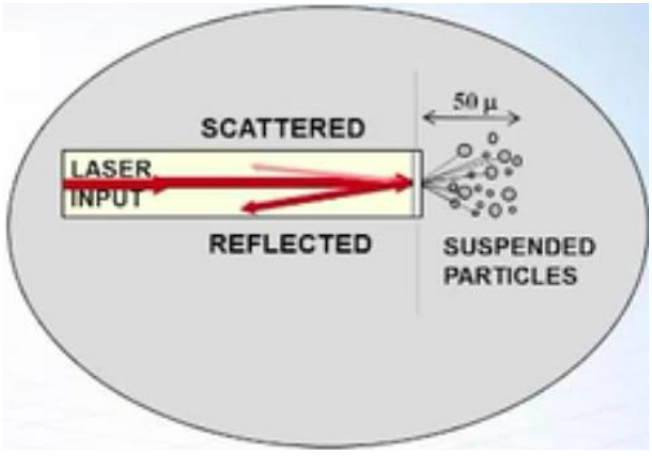

Fig. 15: Schematic representation of the of the operation of the DLS probe [77].

The additives used to perform these experiments were the best nucleation inhibitors found during the crystallization tests from solution (see section 3.1), but added at concentration lower than that at which the nucleation inhibition occurred, in order to study the effect of nucleation inhibitors on particles size.

For DLS analysis, 100 ml of sodium bicarbonate solution including the additives were placed in a jacketed reactor, which was connected to a water bath for the control of the internal temperature, and magnetically stirred at a moderate speed. During slow cooling (0.6°C/min), the probe connected to the DLS was introduced into the reactor. The measurements were conducted every 15 seconds from the beginning and experiments were repeated in triplicate.

At the end of the tests, a small aliquot of precipitate of each solution was taken and subsequently dried in an oven at a temperature of 55 °C. The recovered powders were than observed with a FESEM (see section 2.6 and 3.5).

2.5 Salt weathering test in calcarenitic rocks and Mercury intrusion porosimetry (MIP)

A common method for understanding the mechanics of natural deterioration is to simulate salt weathering dynamics, under controlled laboratory conditions, by submitting samples to various environmental regimes and carrying out imbibition-drying tests [78; 79; 80]. This procedure may give us more details about salt crystallization in natural stones and may help us to gauge the effectiveness of treatments (e.g., use of crystallization inhibitors) for the prevention of salt damage.

Weathering experiments were carried out on 3×3×3 cm samples of Santa Pudia limestone.

Santa Pudia limestone is a detrital sedimentary rock (i.e. formed by debris or solid particles transported by erosive agents into a sedimentary basin, where they are deposited by gravity and subsequently undergo compaction and cementation) extracted in quarries from Granada (Andalusia, Spain). Its own name indicates that it is a calcareous rock. The main mineral is calcite ($CaCO_3$, 90%), while quartz (SiO_2, <10%) and clays (~ 1%, mostly smectite) are accessory minerals [81]. As regard the biological component, it is composed mostly by remains of algae (mainly red), shells of bivalves, serpulids, echinoderms, remains of bryozoans and benthic foraminifera [81]. Santa Pudia is a stone with high porosity ($29.39 \pm 7.60\%$)[81], easy to quarry and carve and with a beautiful tone (white/pale cream), so it has been massively used for the construction of the main monuments in the city of Granada (e.g. Cathedral, San Jerónimo monastery, Chancillería, and Hospital Real). In addition, it has been used as ornamental rock in pinnacles and other sculptural ornaments [82].

The weathering experiments consisted of cycles of 4 h impregnation with 12.0% (w/w) sodium bicarbonate solution at 35 ºC, 90 RH% and drying for 20 h at 10 ºC, 65 % RH in a BINDER VC 4060 climatic chamber (Vötsch Industrietechnik GmbH, Balingen-Frommern, Germany). Under these conditions, $Na_2CO_3 \cdot 10H_2O$ and $NaCO_3 \cdot H_2O$ are the thermodynamically stable hydrated form of sodium carbonate (see section 1.2, Figure 4b). As regard sodium bicarbonate it was found that sodium bicarbonate powder is stable below 76% RH at 25°C and below 48% RH at 40°C, respectively [83].

During the impregnation time, the stones were completely immersed in solution.

Experiments were performed in the presence and in the absence of the most effective additives selected during the crystallization tests from solution (see section 3.1). Three samples for each solution were used.

The duration of the salt weathering tests was 30 days and stones were weighed every day three times a day (at 9:00, 13:00 and 19:00 h), specifically after impregnation and drying steps in each cycle for the all duration of the tests (Figure 16).

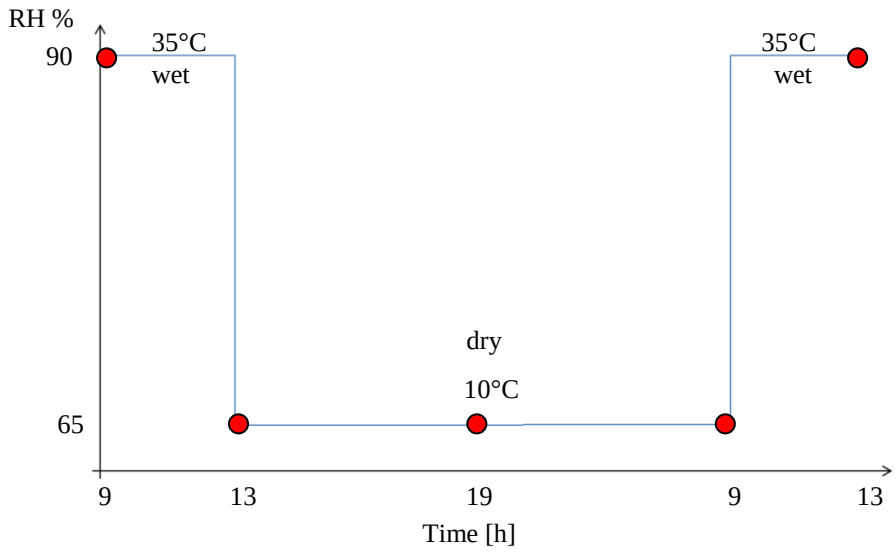

Fig.16: Graphical representation of salt weathering cycle. Red points are the points in which the samples were weighed.

Mass measurements were carried out with a Mettler-Toledo PM4000 technical balance (Mettler-Toledo GmbH, Greifensee, Switzerland) with reproducibility equal to 0.001g.

At the end of the tests, samples were air dried for 5 days. Subsequently, mercury intrusion porosimetry (MIP) was performed both on raw samples and on washed ones, with a Micrometrics Autopore 2500 MIP.

The washing treatment was performed by immersing the stone sample for 15 seconds in a laboratory crystallizer containing MilliQ water. The washing treatment was repeated 3 times per sample. After the washing treatment, samples were air dried for 5 days.

According to the BS ISO 15901-1:2016 standard, sample pre-treatment outside the mercury intrusion porosimeter is not required when the samples are not highly hydrophilic [84], so the samples were not dried in the stove before carrying out the MIP measurements.

Mercury intrusion porosimetry is a widely accepted method for pore size analysis of various materials such as pharmaceutical tablets, building materials, catalysts and their supports, mainly because it allows pore size/porosity analysis to be undertaken over a wide range of pore sizes from meso- to macropores with pore widths from about 0.004 μm to about 400 μm[85]. Since mercury does not wet most substances and does not spontaneously penetrate pores by capillary action, mercury porosimetry describes a non-wetting situation (i.e. the contact angle is greater than 90 degrees) and therefore pressure must be applied to force mercury into the pores.

Accordingly, there is an inverse relationship between the applied pressure, *p*, and the pore diameter, d_p, which, in the simplest case of cylindrical pores, is given by the Washburn equation (equation 13):

$$d_p = \frac{-4\gamma cos\theta}{p} \qquad \text{eq. 13}$$

where γ is the surface tension of mercury (0.480 $N \cdot m^{-1}$), and θ the contact angle that in most cases ranges between 125° and 150° [84].

In the application of mercury intrusion porosimetry, the volume of mercury entering the pore structure is measured as the applied pressure is gradually increased. The value V_{Hg} at the applied pressure *p*, gives the cumulative volume of all available pores of diameter equal to d_p.

The volume of mercury entering the pores is measured by a mercury penetrometer, an electrical capacitance dilatometer (Figure 17). These devices are very sensitive and can detect a change in mercury volume of under 0.1μL.

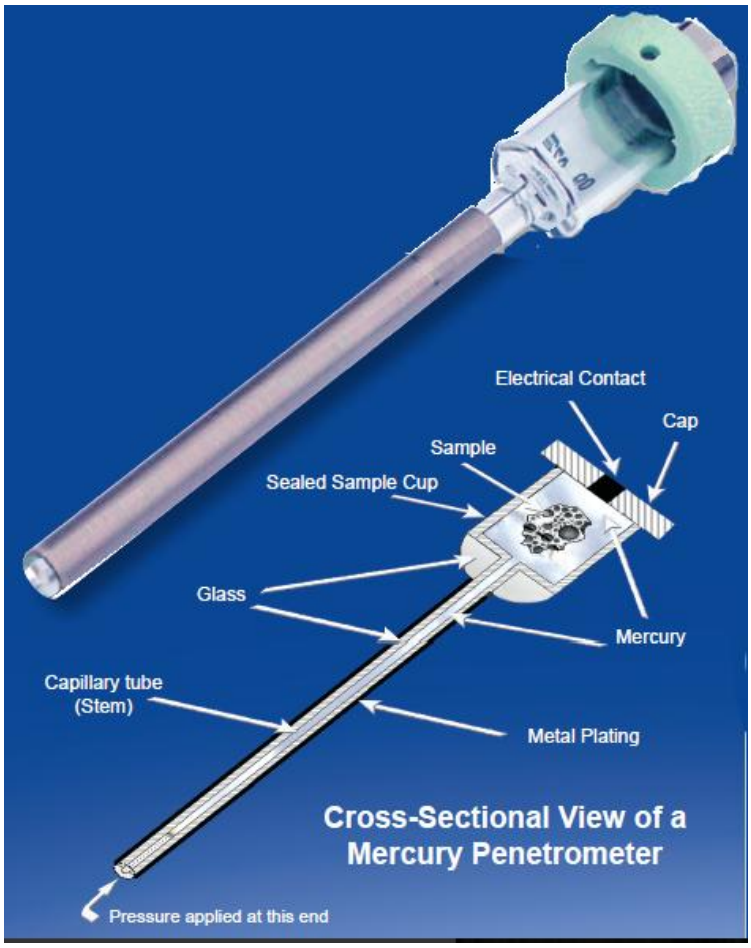

Fig. 17: General and cross section views of a mercury penetrometer [86].

The penetrometer is made of glass (an insulator) and filled with mercury (a conductor). The stem of the penetrometer is a capillary that acts as a reservoir for the analytical volume of mercury. The stem is plated with metal (a conductor). The two conductors, mercury and the metal plating, are separated by glass, thus forming a coaxial capacitor. As pressure forces mercury out of the capillary and into the sample, the mercury inside the capillary decreases and so does the capacitance.

The decrease in capacitance, therefore, is proportional to the volume of mercury leaving the capillary with each change in pressure [84].

In this study, the samples used to perform MIP tests were the ones treated in the climatic chamber and an untreated one (Blank). Stone block were cut with hammer and chisel up to a weight of between 2/ 2.5 grams.

Subsequently the sample is introduced into the mercury penetrometer and then into the porosimeter, where the measurement is carried out. Experiments were repeated in triplicate in order to represent different zones from within the block

2.6 Field Emission Scanning Electron Microscopy (FESEM) investigations

Field Emission Scanning Electron Microscopy (FESEM) is a microscopy technique that provides topographical and elemental information at magnifications of 10x up to 300.000x, with virtually unlimited depth of field. Compared with conventional Scanning Electron Microscopy (SEM), FESEM produces clearer, less electrostatically distorted images with higher spatial resolution [87].

The emitter type (Thermionic emitter for SEM and Field emitter for FESEM) is the main difference between the scanning electron microscope and the field emission scanning electron microscope. Thermionic emitters use electrical current to heat up a filament; the two most common materials used for filaments are Tungsten (W) and Lanthanun Hexaboride (LaB_6) (Figure 18a). When the heat is enough to overcome the work function of the filament material, the electrons can escape from the material itself. Thermionic sources present relative low brightness, evaporation of cathode material and thermal drift during operation. Field Emission is one way of generating electrons that avoids these problems. A Field Emission Gun (FEG), also called cold cathode field emitter, does not heat the filament. The emission is reached by placing the filament in a huge electrical potential gradient. The FEG is usually a wire of Tungsten (W) fashioned into a sharp point (Figure 18b) [88].

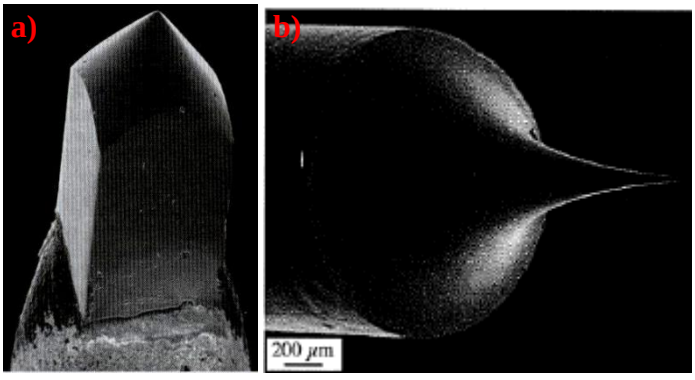

Fig. 18: a) An LaB_6 crystal, **b)** W crystal sharpened to a tip radius of about 100 nm [88].

This increases the density of the beam and also the beam is energetically more coherent. The increase of the beam density increases significantly the brightness of the images that is very convenient when it is necessary to decrease the spot size (to increase the

resolution) or to decrease the accelerating voltage (to see more details of a surface). Coherency of the energy is very important because the beam has to cross the magnetic fields of the lens and all the electrons are supposed to follow the same way for the same initial conditions. Incoherency of the beam increases aberration and decrease resolution, particularly at low accelerating voltage [87].

In this work a FESEM Carl Zeiss Auriga model was used. The analysis with FESEM allowed us to study the morphology with which nahcolite, natron and thermonatrite precipitate, in the presence and in the absence of a calcitic support.

The samples analyzed without a support were the crystals obtained after the crystallization tests from solution (see section 2.2), both for the control solution and the solutions with additives.

As regard the crystals obtained from the solutions with additives, the additives used were the nucleation inhibitors selected during the crystallization tests from solution but used at concentration lower than that at which the nucleation inhibition occurred (see section 3.1).

In order to visualize the change of morphology due to the effect of additives with respect to the control solution, a small aliquot of precipitate of each solution was taken at the end of the crystallization tests from solution and subsequently dried in an oven at a temperature of 55°C.

Subsequently, recovered powders were attached to a sample holder with a carbon adhesive tape. After that, samples were carbon coated.

Two different calcitic supports were also used to study the crystallization of carbonates in the presence and in the absence of additives: (i) freshly cleaved Iceland Spar single crystals (ca. 2 × 3 × 5 mm sized) and (ii) pieces taken from stone blocks of Santa Pudia limestone (see section 2.5).

A 100 μL drop of saturated $NaHCO_3$ solution, with and without additives, was placed on a calcite crystal and let evaporate in a room at 23°C, RH 39.8%.

Additives used were the crystallization modifiers selected after the crystallization tests from solution (see section 3.1).

Subsequently, calcite crystal were attached to a sample holder with a carbon adhesive tape. After that, samples were carbon coated.

As regards the supports made of Santa Pudia limestone, fragments were obtained from the raw stone used for MIP tests (see section 2.5).

Fragments were attached to a sample holder with a carbon glue. After that, samples were carbon coated.

3. Results and Discussion

3.1 Effectiveness of crystallization modifiers

Regardless of the presence or absence of additives, the white powder precipitated following *T* decrease during crystallization in solution tests (Figure 19) was identified as nahcolite ($NaHCO_3$) and natron ($NaCO_3 \cdot 10H_2O$) by XRD analyses (see section 3.2).

Fig.19: Precipitate recovered during crystallization tests.

It is possible to say that all the different tested additives acted as inhibitors of the crystallization of sodium bicarbonate when they were added to saturated solution of sodium bicarbonate at pH 7.9, because the critical supersaturation (i.e., supercooling) achieved, expressed as the difference between the equilibrium Temperature (T_{eq}) and the crystallization Temperature (T_{cryst}), for the additive concentrations used (0,1; 1; 10 mM) was higher than that of the control solution (Figure 20).

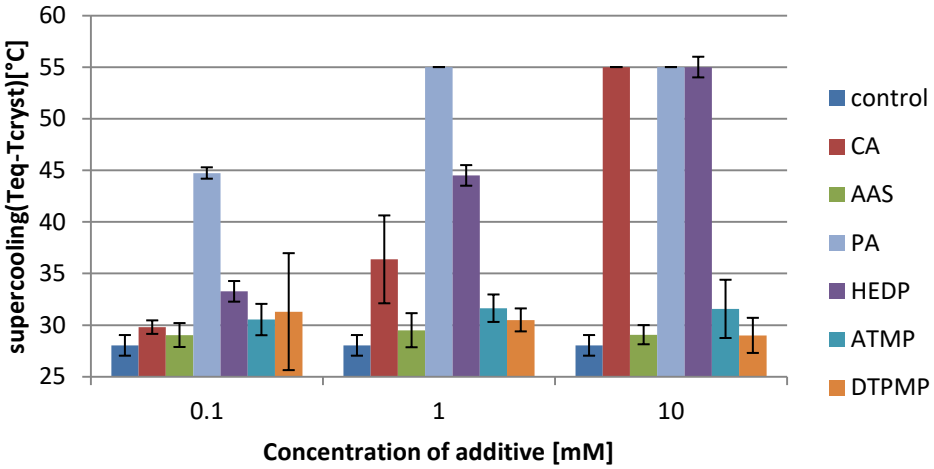

Fig.20: Difference between the equilibrium Temperature (T_{eq}) and the crystallization Temperature (T_{cryst}) of a saturated solution of $NaHCO_3$, with and without (control) selected organic additives. Values are average of three replicates; error bars indicate standard deviation.

For AAS, ATMP and DTPMP it is possible to say that they don't show a great effect as inhibitors, because their differences between the equilibrium and the crystallization temperature do not significantly differs from that of the control.

For PA, CA and HEDP it is possible to say that, increasing their concentration in the solution, their inhibitory capacity increases up to the complete inhibition of the crystallization of sodium bicarbonate. As regards PA, at our operating conditions (see section 2.2), crystallization does not occur anymore already at a concentration equal to 1 mM, while for CA and HEDP crystallization is not observed at concentrations equal to10 mM. Hence, PA seems to be the best inhibitor, as it allows to completely inhibit the crystallization of sodium bicarbonate at a low concentration of additive tested (1 mM).

It should be noted that when PA was used at a concentration of 0.1 mM, during the cooling process, the solution began to acquirer opalescent coloration at about 10 °C, however without leading to the formation of any recoverable precipitate. The latter was obtained after maintaining the solution at 2°C for about 15 minutes, in order to increase the supersaturation of the system and provide the system enough energy to crystallize (i.e., to enable the coalescence/growth of the initial colloidal precipitates).

Overall, in the presence of the additives, the onset of crystallization is delayed and the lag or waiting time increased as the additive concentration increased [6; 45].

To compare the best inhibitors and evaluate their efficacy according to the concentration used to obtain maximum inhibition under our operating conditions, the critical supersaturation data were normalized with respect to the control critical supersaturation by using the "*percentage of growth inhibition"* (G.I)[89], calculated using equation 14:

$$G.I = \frac{\sigma_{additive} - \sigma_{control}}{\sigma_{control}} \cdot 100 \qquad \text{eq.}$$

where $\sigma_{additive}$ and $\sigma_{control}$ are the critical relative supersaturations in the presence and in the absence of the additive, respectively, calculated with PHREEQC. In the absence of additives, the critical supersaturation σ_{contol} was found to be 0.73 ± 0.032. Critical supersaturations were calculated at a constant pH of 8.2. This simplification was possible because the pH variation during crystallization tests was found to be not significant for all runs (the pH of the solutions generally increased from 7.9/8.1 of the starting solution to 8.3/8.5 of the ending solutions). Results shown in Figure 21 confirm what was already observed. For CA, PA and HEDP, there is a clear tendency to increase the percentage of inhibition associated with the additive concentration, and PA results the best inhibitor as it can completely interrupt the crystallization of sodium bicarbonate when used at a

concentration of 1mM. As reported in other studies, this may be due to a higher degree of coverage of the crystallization embryo by the additive [5; 6].

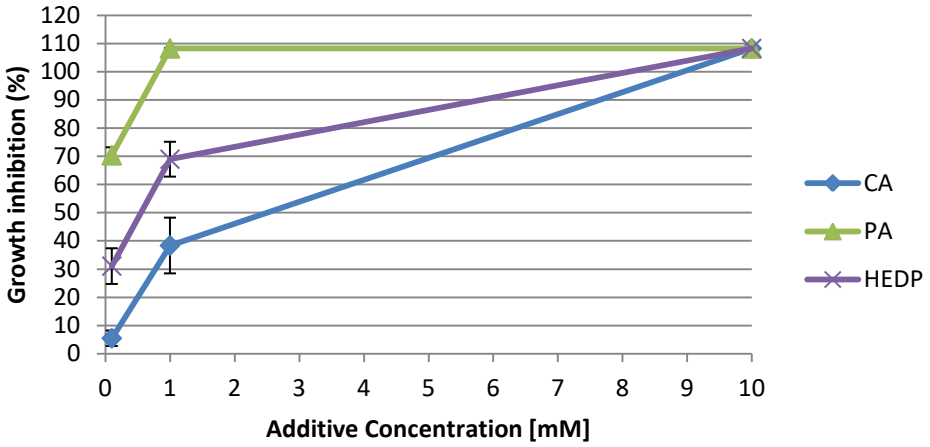

Fig. 21: Percentage of growth inhibition vs. inhibitor concentration (at pH 8.2) for saturated sodium bicarbonate solutions. Values are averages of three replicates; error bars indicate standard deviations.

Regarding the pH effect, on the basis of previous research [5; 6; 45; 52; 65], the mechanism of nucleation inhibition in the presence of organic additives can be explained by the electrostatic attraction generated between the deprotonated organic additives and the cations present in solution or forming prenucleation ion-associates (i.e., prenucleation clusters) (see section 1.4). Accordingly, the strong dependence of organic inhibitors on pH is evident. Figure 22 shows the distribution of the ionic species for the different additives as a function of pH [5; 6] calculated from published pKa values reported in table 5 [90; 91; 92; 93].

	CA[a]	AAS[b]	PA[c]	HEDP[a]	ATMP[a]	DTPMP[d]
-log K_1	5.43	9.60	4.5	11.0 ± 0.2	12.5 ± 0.2	12.58
-log K_2	3.81	3.65		6.9± 0.1	7.22± 0.03	11.18
-log K_3	1.82	1.88		2.7±0.1	5.90±0.02	8.30
-log K_4				1.6±0.2	4.59±0.03	7.23
-log K_5					12.5 ± 0.2	6.23
-log K_6					1.6± 0.3	5.19
-log K_7					0.5±0.3	4.15
-log K_8						3.11
-log K_9						2.08
-log K_{10}						1.04

Tab. 5: Protonation constants of CA, AAS, PA, HEDP, ATMP and DTPMP.

[a] data from reference [90]; [b]data from reference [93]; [c] data from reference [92] ; [d]data from reference [91].

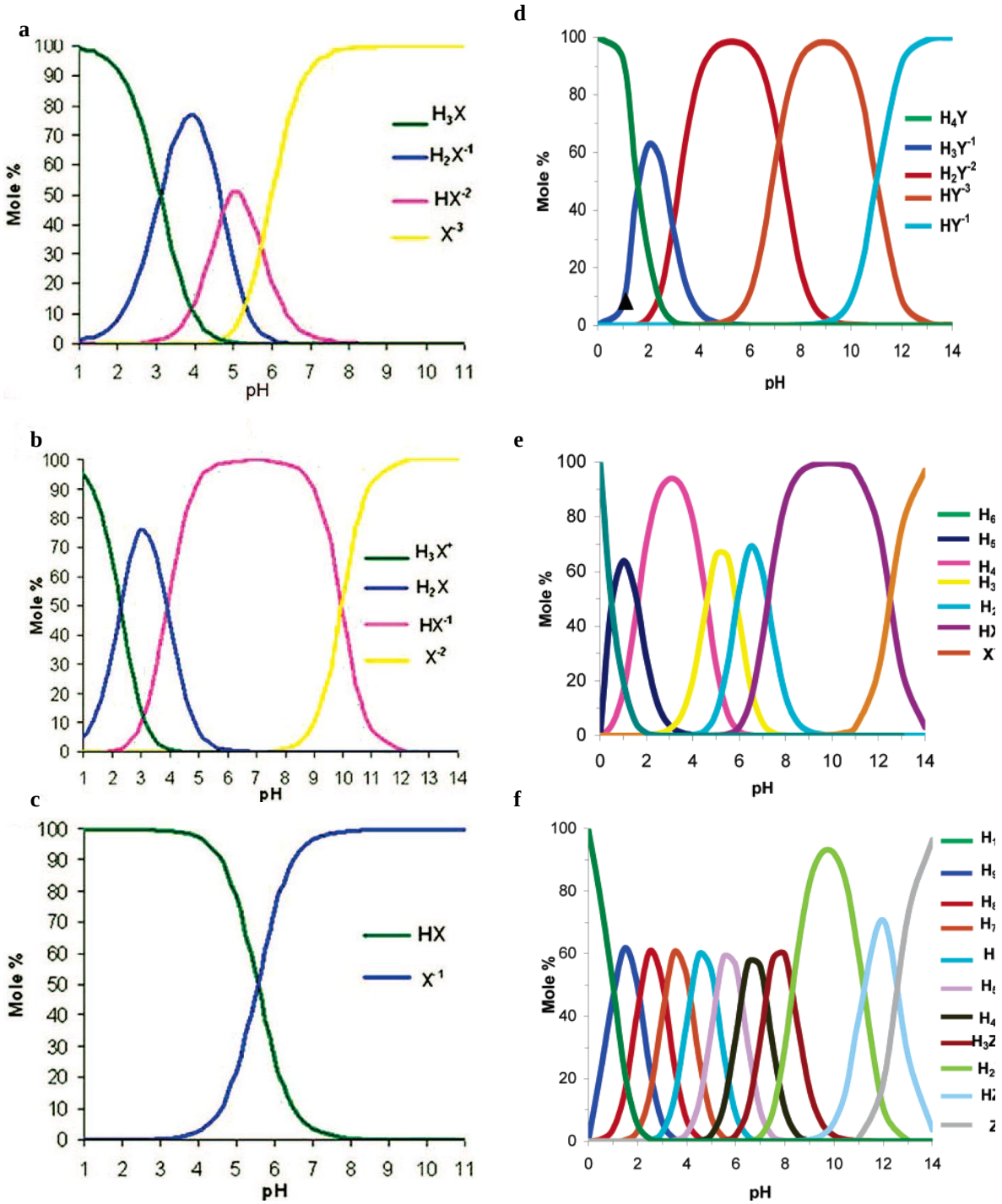

Fig. 22: Distribution of ionic species as a function of pH: **a)** CA, **b)** AAS, **c)** PA, **d)** HEDP, **e)** ATMP, **f)** DTPMP [5; 6].

As shown in Figure 21, in all cases functional groups in the inhibitor molecules tested are highly deprotonated at pH 8-8.5, that is, the pH range of the solutions.

The inhibitor capacity of CA can be due not only to a higher percentage of surface coverage by additive as concentration increases but also to the fact that at pH 8 the molecule has three deprotonated functional groups. This allows the citrate to interact

with the cations both free in solution or incorporated in the pre-nucleation clusters (see section 1.4) and prevent the crystallization of sodium bicarbonate.

On the contrary, the inefficiency of AAS as a crystallization inhibitor may be due to the fact that aspartic acid possesses only two deprotonated functional groups in the pH range of interest. Therefore, crystallization embryos, with a size below the critical size, at all additive concentrations, are not effectively bounded by the deprotonated acid, so they can aggregate and crystallize.

As regards PA, at pH 8 the polymer is completely deprotonated and has great stabilizing effect on sodium bicarbonate crystallization embryos. This seems to be ascribable to the strong interaction between the deprotonated carboxylic groups in the macromolecule side chain and cations in the embryos. Moreover, it was reported in other studies [94] that the stronger stabilizing effect of PA may be attributed to the larger decrease in molecular mobility of ions in solution induced by this additive.

As regards ATMP and DTPMP, the obtained results show that despite the fact that these phosphonates are highly deprotonated at the pH of interest, they are ineffective as nucleation inhibitors for sodium bicarbonate. This could be attributed to the fact that ATMP and DTPMP molecules are very large and branched, so that steric effects could worsen the adsorption of these molecules on the surface of the crystallization embryos, which then aggregate and crystallize.

Conversely, HEDP, which contains only two phosphonate groups and at pH 8 is less deprotonated than the other two phosphonates tested, is effective as nucleation inhibitor at a concentration of 10 mM.

The HEDP molecule is smaller and less branched than the molecules of the other two phosphonates, and this could confirm the previous hypothesis on the inefficacy of ATMP and DTMP as nucleation inhibitors.

Therefore, the effectiveness of a phosphonate to inhibit crystallization of salts would not appear to be based exclusively on electrostatic interactions. Apparently, the degree of structural matching between inhibitor and crystal embryo surfaces seems to be particularly important [5].

3.2 Phase identification

Using XRD, we identified the formation of different solid phases during the crystallization tests in solution (see section 3.1) and the evaporation tests performed using the zero background silicon sample holders (see section 2.3). These results, combined with the thermodynamic study carried out with PHREEQc (see section 2.2) and the calculation of the nucleation density (see section 3.3), allowed us to make some observations about the order in which the phases are formed and the reasons that lead to their (sequential) formation.

As reported in the previous section, nahcolite ($NaHCO_3$) and natron ($NaCO_3 \cdot 10H_2O$) were the only phases that precipitated during the cooling-induced crystallization tests.
In Figure 23 it is shown the XRD pattern of solids recovered after sodium bicarbonate solution crystallization in the absence of additives. The patterns obtained in the presence of additives do not differ, so they are not reported. In table 6 the percentage amount of both phases is shown for each run.

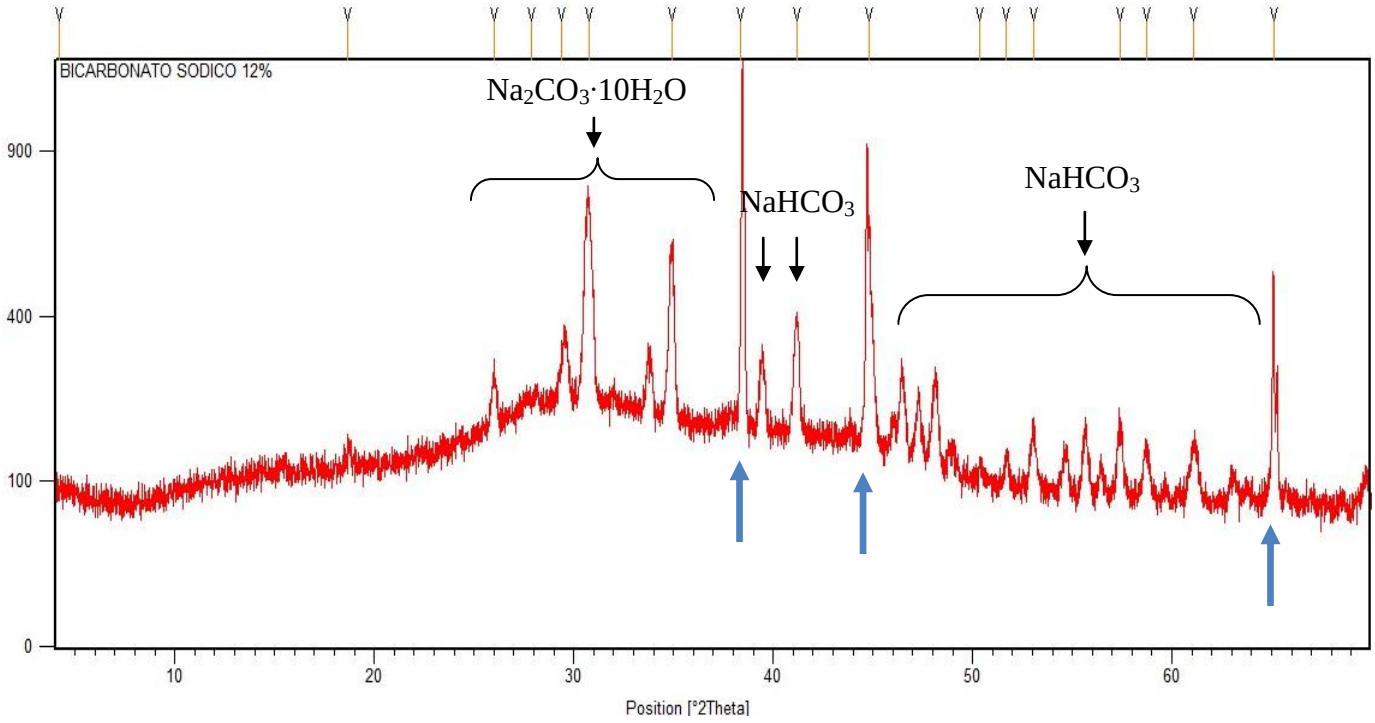

Fig. 23: XRD pattern of solids formed after crystallization of a sodium bicarbonate solution in the absence of organic additives. Scan time: 10 min. Sample holder: aluminum (peaks marked with blue arrows: 38.54 deg, 44.83 deg, 65.18 deg).

SOLUTION	Control	CA			AAS			PA			HEDP			ATMP			DTMP		
ADDITIVE CONCENTRATION [mM]	0	0,1	1	10	0,1	1	10	0,1	1	10	0,1	1	10	0,1	1	10	0,1	1	10
NAHCOLITE[%w/w]	48	50	23	-	85	77	68	55	-	-	52	52	-	50	71	64	48	48	32
NATRON[%w/w]	52	50	77	-	15	23	32	45	-	-	48	48	-	50	29	36	52	52	68

Tab. 6: Percentage amount of natron and nacholite in the filtrate [%w/w], determined through XRD. "-" means that no precipitation was reached at the temperature of 2°C. Quantitative analysis performed using the computer code X'Pert High Score (RIR method).

As regards the evaporation tests on the silicon substrate, the two phases formed at the end of the tests were thermonatrite ($Na_2CO_3 \cdot H_2O$) and nahcolite ($NaHCO_3$) for all the samples (control, CA 10 mM, PA 1 mM, HEDP10 mM).

In Figure 24 the XRD pattern collected at the end of the evaporation test for the control solution is shown. The patterns obtained in the presence of additives do not change, so they are not reported here.

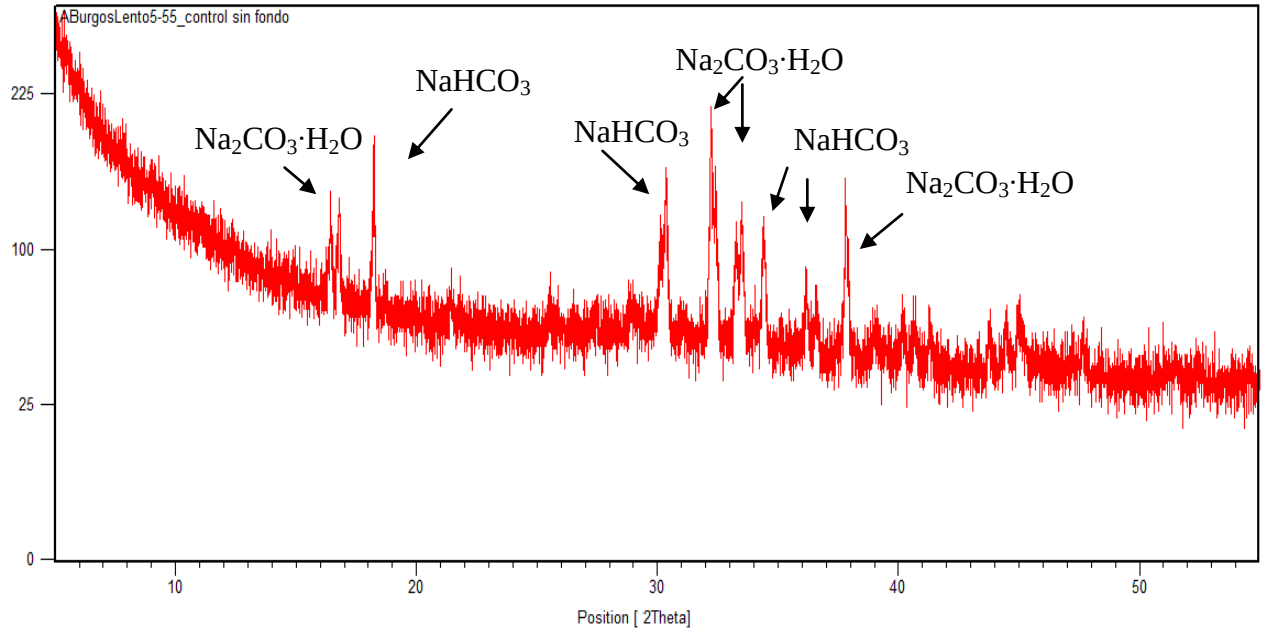

Fig. 24: XRD pattern of sodium bicarbonate crystallization in the absence of additives by evaporation tests on a silicon substrate. Scan time: 55 min.

In Figures 25, 26, 27, and 28 the diffractograms obtained for the samples during all the evaporation tests are shown.

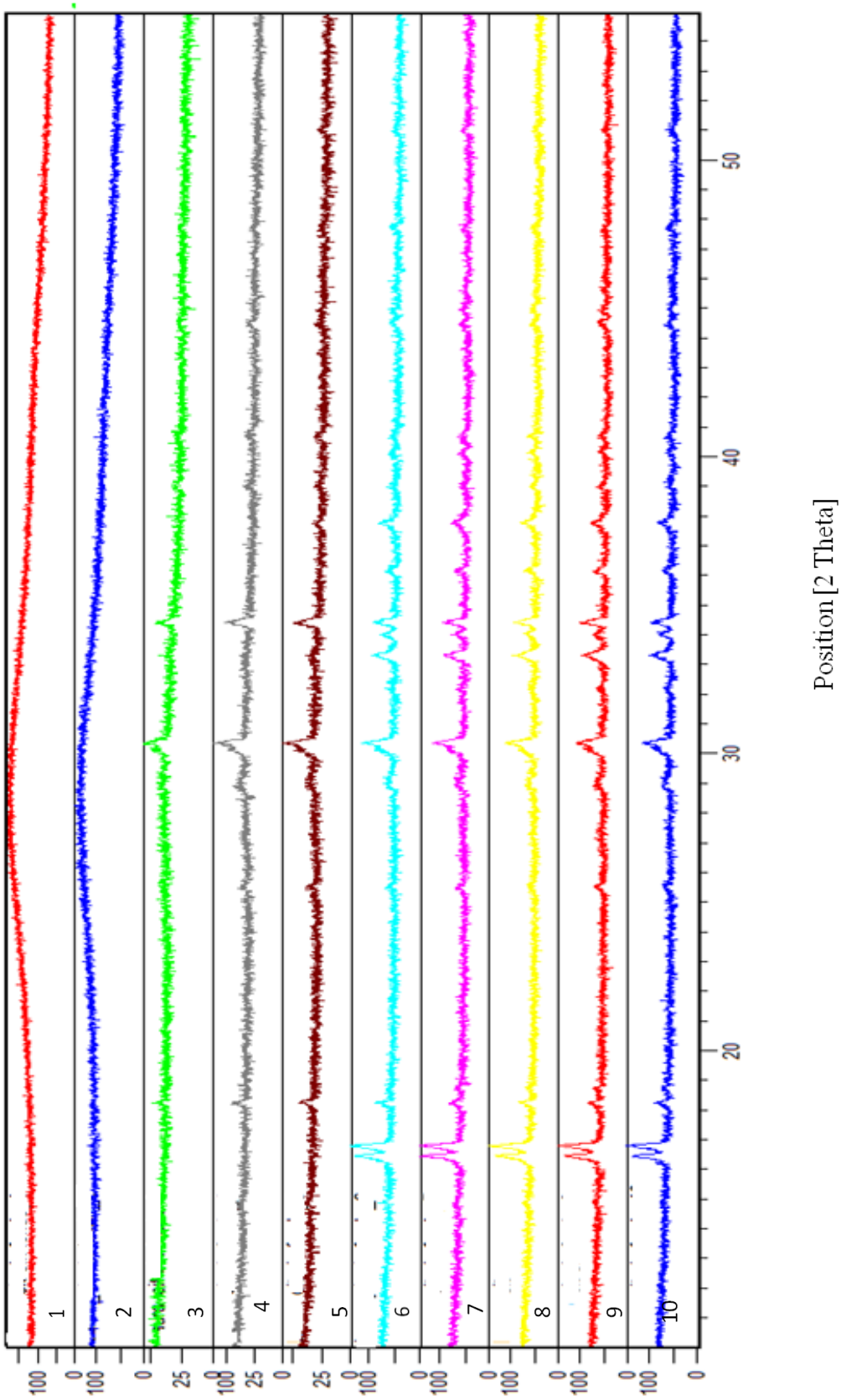

Fig. 25: Time-resolved XRD patterns for sodium bicarbonate crystallization in the absence of additives by evaporation on a silicon substrate. Scan time for patterns from 1 to 9: 7 min. Scan time for pattern 10: 55 min.

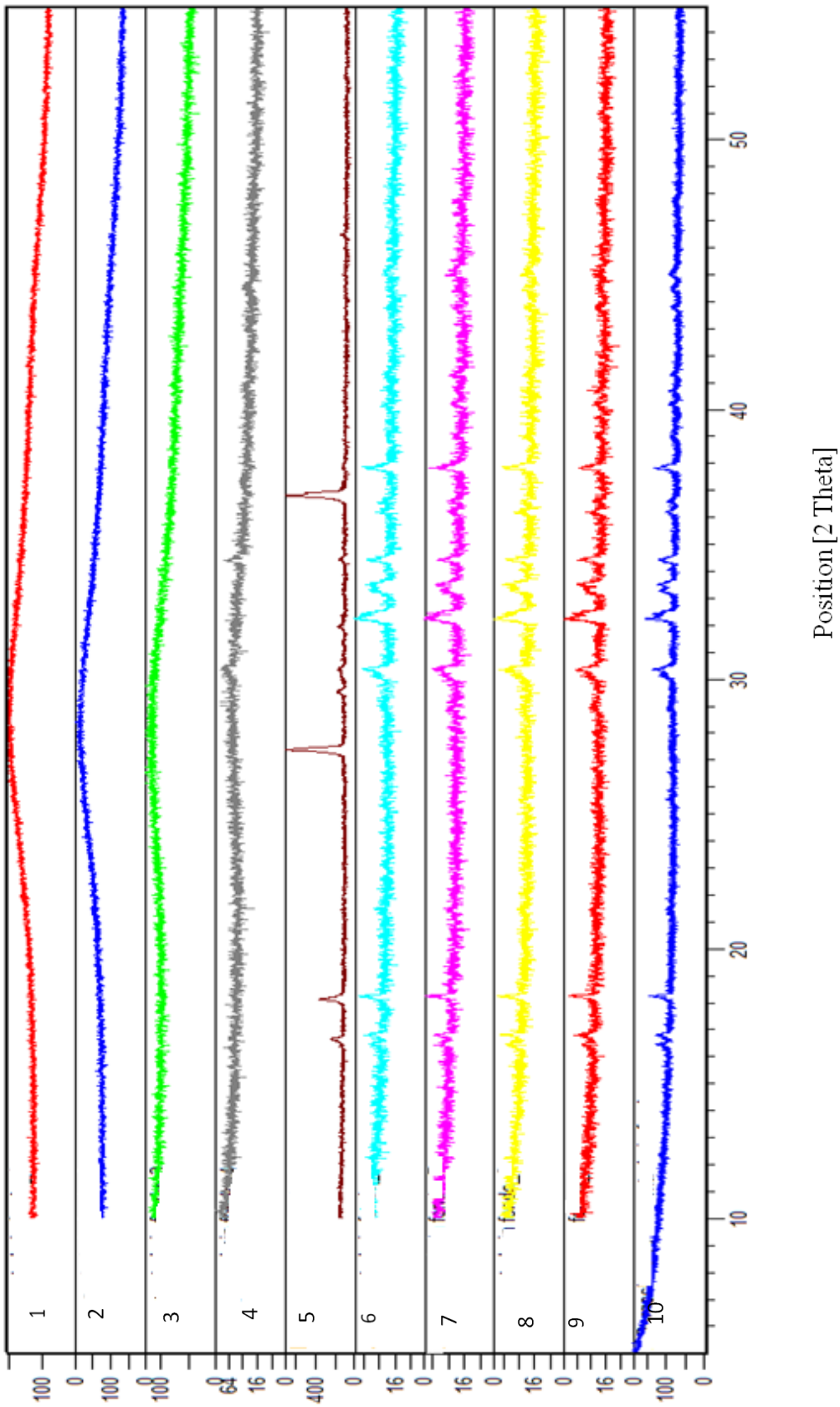

Fig. 26: Time-resolved XRD patterns for sodium bicarbonate crystallization in the presence of 10 mM CA by evaporation on a silicon substrate. Scan time for patterns from 1 to 9: 7 min. Scan time for pattern 10: 55 min.

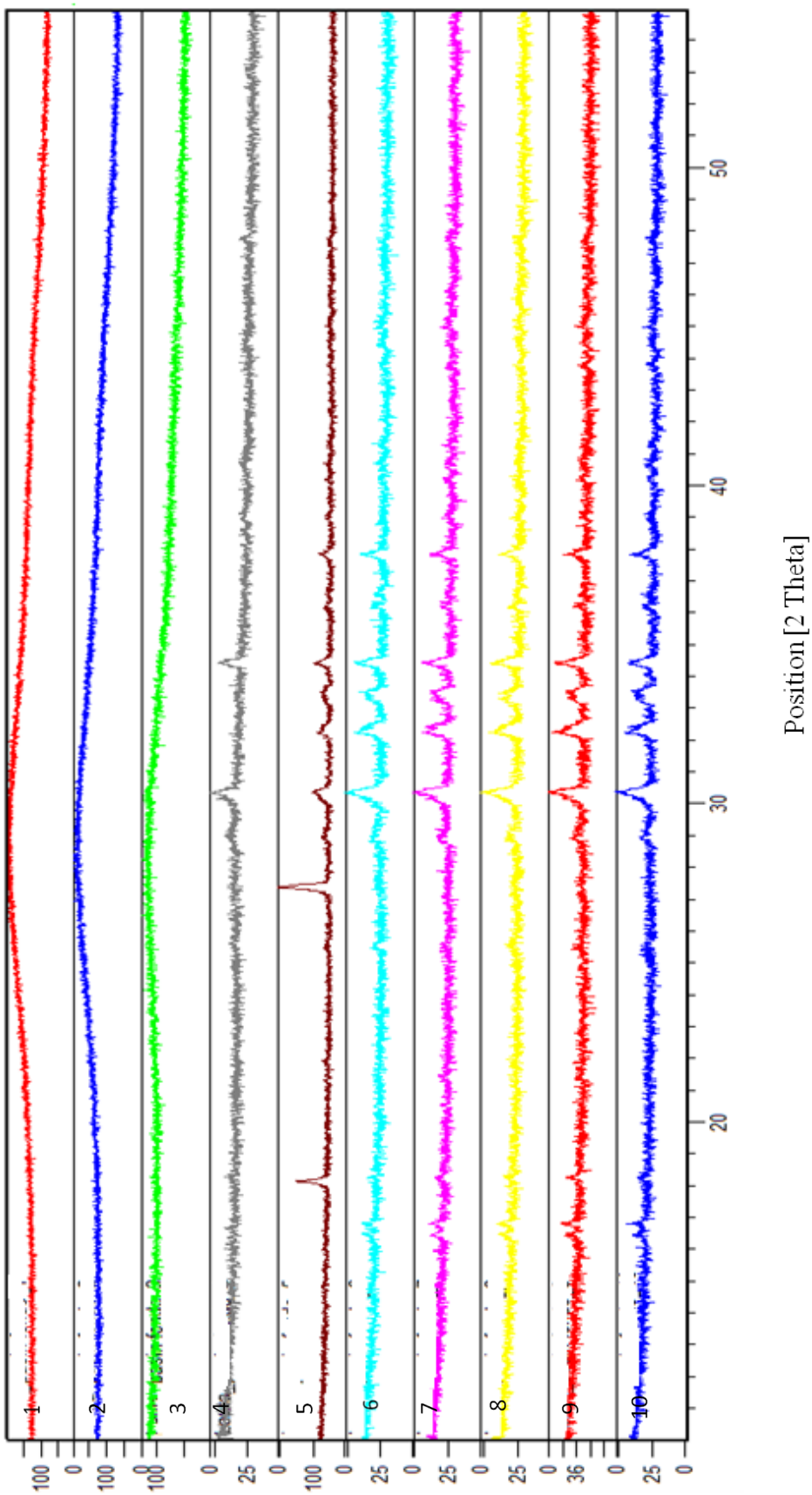

Fig. 27: Time-resolved XRD patterns for sodium bicarbonate crystallization in the presence of 1 mM PA by evaporation on a silicon substrate. Scan time for patterns from 1 to 9: 7 min. Scan time for pattern 10: 55 min.

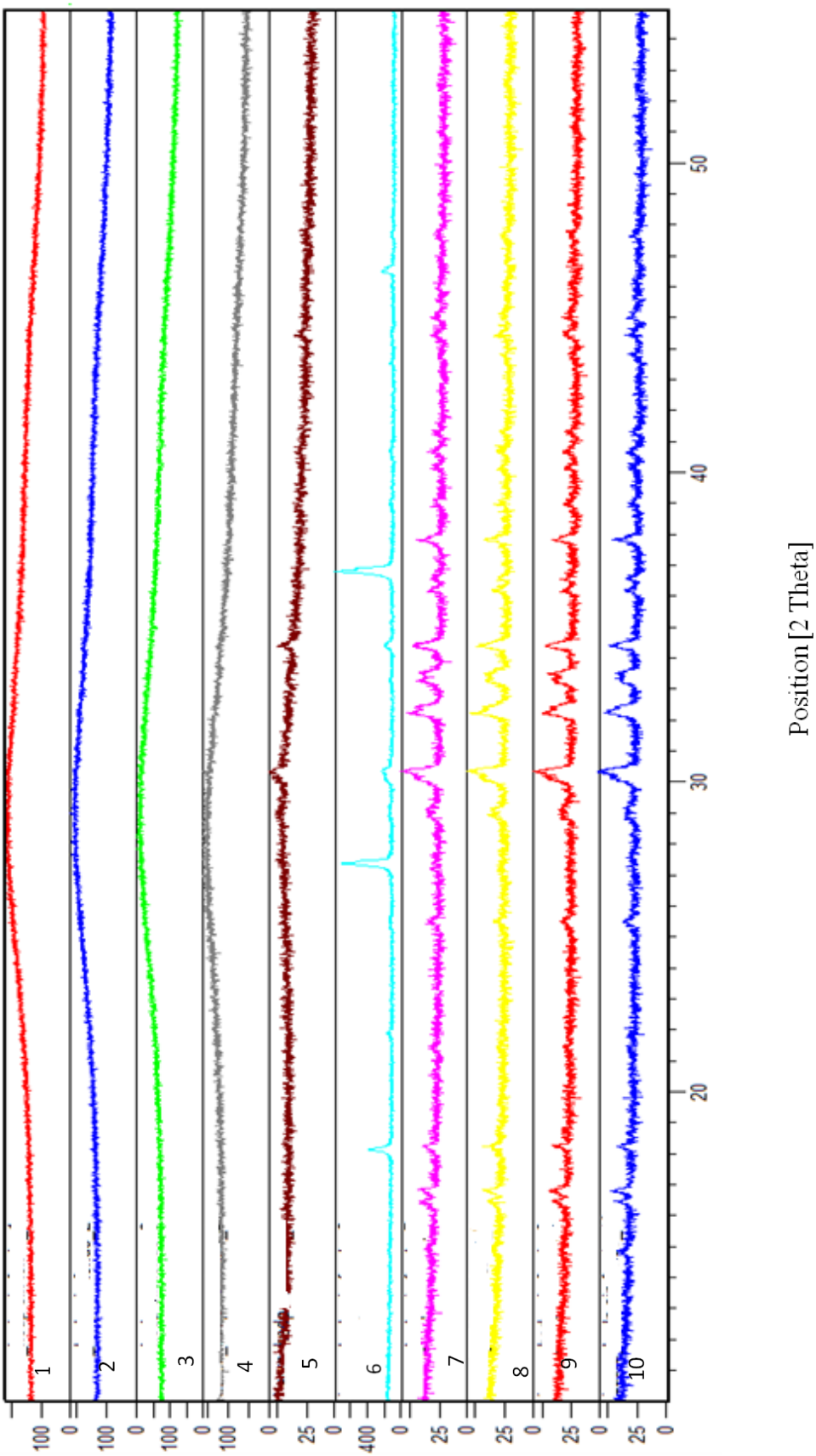

Fig. 28: Time-resolved XRD patterns for sodium bicarbonate crystallization in the presence of 10 mM HEDP by evaporation on a silicon substrate. Scan time for patterns from 1 to 9: 7 min. Scan time for pattern 10: 55 min.

It is interesting to note that during both tests (cooling-induced and evaporative crystallization) and in the case of all samples, the presence of natron or thermonatite, respectively, was detected after the nucleation of nahcolite.

More specifically, during crystallization tests in solution (induced by a drop in *T*) the presence of natron was detected at the end of the analysis (i.e. when the temperature reached 2°C and the pH was around 8.3/8.5), but, on the basis of PHREEQC modeling, such a phase should not form at the crystallization temperature, except for 0.1 mM PA and 1 mM HEDP, which crystallize at about 10°C (pH 8.3-8.4). Actually, PHREEQC modeling shows that in a range of pH of 8.0-8.2 and for temperatures above 15°C, nahcolite is the only thermodynamically possible phase.

During the evaporation tests, the presence of thermonatrite was detected after the formation of nahcolite. More specifically, it was detected 42 minutes after the beginning of the analysis for control, CA and PA, and after 49 minutes for HEDP, while the formation of nahcolite was detected after 14 minutes for the control, after 21 minutes for CA and PA, and after 35 minutes for HEDP.

This phenomenon could have three possible explanations, some of them likely acting simultaneously.

The first explanation is related to the fact that $NaHCO_3$ starts to break down at temperatures well below 323 K in open air [95; 96] according to the following reaction:

$$2Na_2HCO_{3(s)} \leftrightarrow Na_2CO_{3(s)} + H_2O_{(l)} + CO_{2(g)} \quad (1)$$

This implies that during the preparation of the sodium bicarbonate solution a small amount of sodium carbonate, generated by reaction (1), may be also introduced.

The latter may have led to the crystallization of its more or less hydrated forms depending on the experimental conditions at which the two tests were conducted (see sections 2.2, 2.3). So, during the crystallization tests in solution (RH 100%, controlled cooling from 55 to 2°C), the formation of natron, the decahydrate phase, would be favored (see section 1.2, Figure 4b). During the evaporation tests the formation of the monohydrate phase of sodium bicarbonate would probably be due to the smaller quantity of water in the system (100μL) with respect to the batch one (88 mL) and to the low RH found in our laboratory (38.9% RH, 23°C). These conditions make highly unlikely that any phase other than thermonatrite would crystallize (see section 1.2, Figure 4a). The

problem with this hypothesis is that if any sodium carbonate seed would be present, then the first phase to form would be the sodium carbonate phase (either natron or thermonatrite). But this is not what we observed: from the evaporative crytallization tests we see that the first phase formed is nahcolite. In summary, this first hypothesis does not seem to explain our experimental results.

The second possible explanation is that some reactions [97; 29] occur that lead to the formation of thermonatrite from nahcolite through the formation of trona ($2Na_2CO_3 \cdot NaHCO_3 \cdot 2H_2O$).

$$3NaHCO_{3(s)} + H_2O_{(l)} \leftrightarrow Na_2CO_3 \cdot NaHCO_3 \cdot 2H_2O_{(l)} + CO_{2(g)} \quad (2)$$

$$2Na_2CO_3 \cdot NaHCO_3 \cdot 2H_2O_{(s)} \leftrightarrow 3Na_2CO_3 \cdot H_2O_{(s)} + 2H_2O_{(l)} + CO_{2(g)} \quad (3)$$

Reaction (2) occurs above 21°C [98] while reaction (3) has been experimentally investigated at both high P-T conditions [96] and low P-T conditions [97] and has been observed when the level of carbon dioxide is very low (Figure 29).

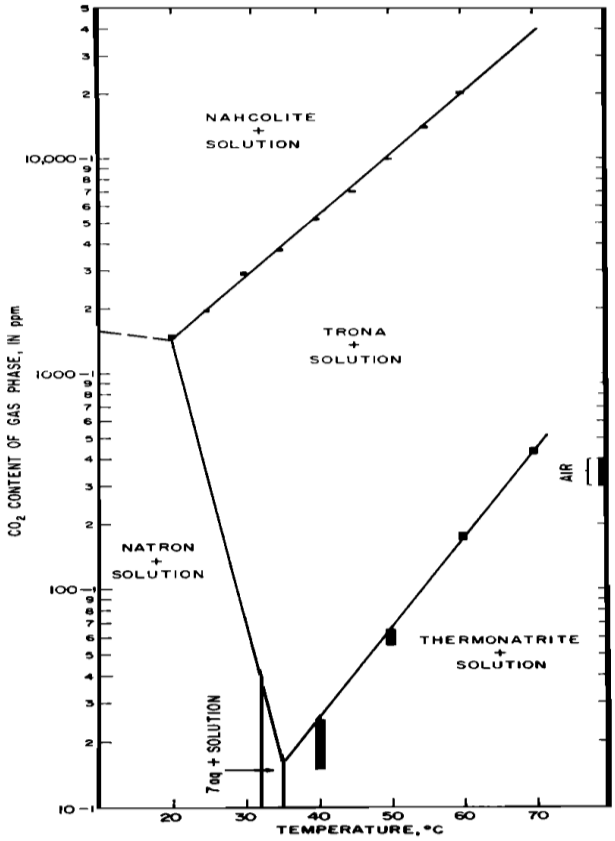

Fig.29: Stability fields of sodium carbonates as a function of CO_2 content (in ppm) of gas phase vs. temperature. The range labeled 'AIR' represents the range of atmospheric CO_2 content for reference [97].

Therefore, during the crystallization tests in solution the formation of trona could take place as a result of the formation of nahcolite (reaction (2)), followed by the formation of natron which, as already stated, forms at low temperatures and high RH conditions (see section 1.2, Figure 4b).

As for the evaporation tests, trona presence was not detected during the collection of XRD patterns. This may be due to the fact that the experimental conditions did not allow the stabilization of this phase, thus leading to the immediate formation of thermonatrite.

The third explanation of the phenomenon can be rationalized on the basis of the equilibria and speciation of carbonic acid.

When sodium bicarbonate is dissolved in milliQ water at 55°C to prepare the saturated saline solution (pH 7.9), the reaction is the following:

$$NaHCO_{3(s)} \leftrightarrow Na^{+}_{(aq)} + HCO^{-}_{3(aq)} \qquad (4)$$

During the crystallization tests in solution the temperature of the bath is lowered to 2°C (see section 2.2).

Lowering the temperature, the solubility of the system decreases. Therefore, at the crystallization temperature, sodium and bicarbonate ions will aggregate and shift the balance of reaction (4) to the left, causing nahcolite precipitation.

As precipitation of nahcolite continues, the system will tend to slightly basify resulting in the formation of a small amount of carbonate ion (Figure 30) due to the dissociation of the bicarbonate ion. The reaction is the following:

$$HCO_3^- \leftrightarrow CO_3^{2-} + H^+ \qquad (5)$$

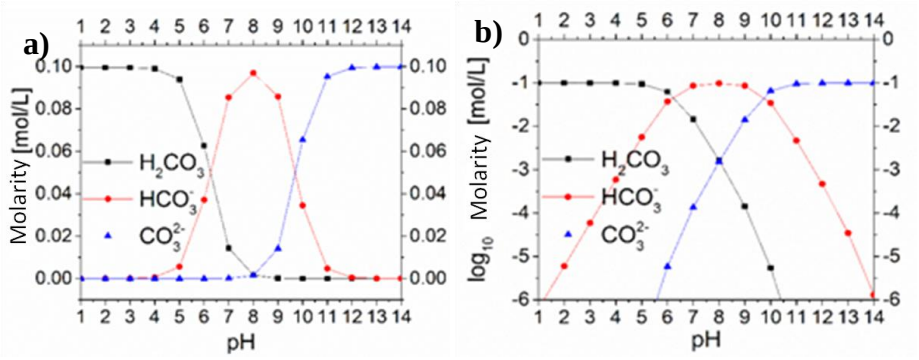

Fig. 30: Distribution of carbonate species in water as a function of pH of the solution at 25°C. The graphs have been made with PHREEQC, **b)** represents the same information of **a)** but in logarithmic scale.

Furthermore, by cooling the system, the solubility of carbon dioxide, contained in the dead volume of the reactor, increases, according to the following reactions:

$$CO_2 + H_2O \leftrightarrow H_2CO_3 \leftrightarrow HCO_3^- + H^+ \leftrightarrow CO_3^{2-} + 2H^+ \quad (6)$$

Once dissolved, it can lead to the production of further carbonate ions and the carbonation of the system.
It should also be specified that the solution comes into contact with the air during the inserting/removal of probes and the filtering operations.
Under these evolving conditions of temperature, relative humidity, pH, and CO_2 content, the most likely phase of sodium carbonate that should crystallize (after nahcolite) is natron (see section 1.2, Figure 4b).

During the evaporation tests the reactions that probably occur in the system are the same seen previously. It must be considered that the solution drop is evaporated in a rotating silicon plate, so the exposure time to air and the consequent accumulation of CO_2 in the system will be higher compared to the batch system.
As already stated, the formation of the monohydrate phase instead of the decahydrate phase is due to the smaller quantity of water in this system than in the batch one and to the low RH found in our laboratory (38.9% RH, 23°C).

There is, finally, another alternative hypothesis to explain why natron could precipite after nahcolite in the crystallization from solution tests (although this was not directly proved due to our experimental set up that prevented us from collecting precipitates formed during the very early stages of crystallization). This hypothesis is related to the differences in interfacial energy between the two phases, leading to significant variations in nucleation density at equal supersaturation values. This hypothesis is developed in the following section.

3.3 Determination of nucleation density and growth analysis

By determining the nucleation density it was possible to confirm the results obtained by PHREEQC regarding the crystallization from solution tests and to determine the phase precipitation sequence.
Using DLS, it was observed that the inhibitors selected in the first part of the study, i.e., those with the highest inhibition (CA, PA, HEDP), used at concentration lower than that at which complete nucleation inhibition occurred (1mM, 0.1mM, 1mM, respectively) acted on the growth of the particles by reducing their size.
These results, combined with the images obtained using FESEM (see sections 2.6 and 3.5), allowed us to make some observations about the way in which inhibitors acted.

A critical parameter to determine the nucleation density (and the effects additives have on this important parameter) is the surface tension or surface energy (also called interfacial energy or interfacial tension) of a solid phase. As no experimental values were found for nahcolite and natron surface tension, a rough estimation was made by an analytical expression (equation 15) given by Söhnel in 1981 [39], where the surface tension is expressed as a function of substance solubility:

$$\gamma = -20 \log c_{eq} + 32 \qquad \text{eq.15}$$

where c_{eq} is the solubility of a given substance at 20°C, selected from reference [99]. Hence, γ of nahcolite equals 0.037 N/m and that of natron is 0.043 N/m.
According to what was reported by Söhnel in 1981[39], these values are attributable to soluble salts (Figure 31).

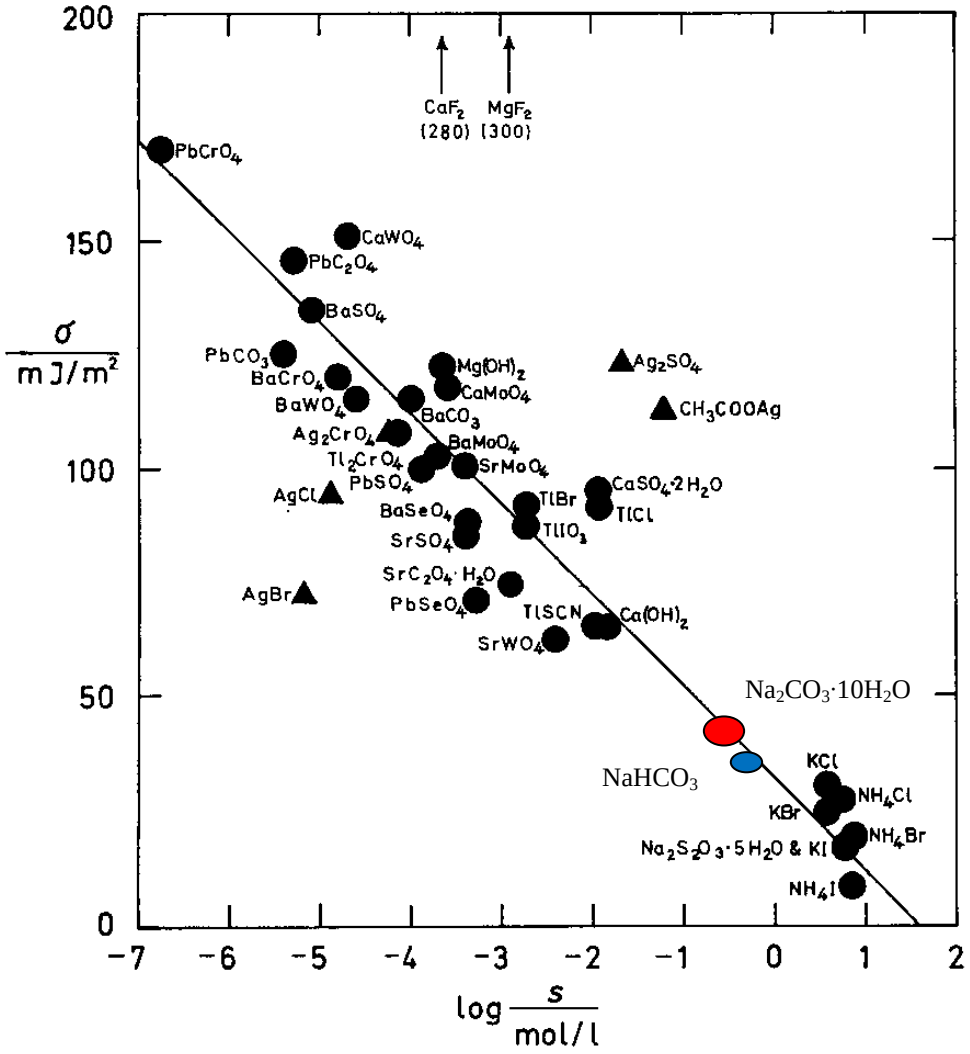

Fig.31: Interfacial tension between crystal and aqueous solution as a function of the logarithm of the solubility. Natron in red, nahcolite in blue. Image modified from reference [39].

The obtained values were used to calculate the nucleation density of nahcolite and natron through equation 6 (see section 1.3). Figure 32 shows the results calculated at 20°C and plotted as a function of the supersaturation index (β), expressed as the ratio between molality, c, and solubility, c_{sat} [99].

In table 7 supersaturation indices and nucleation density values of the four solutions are reported.

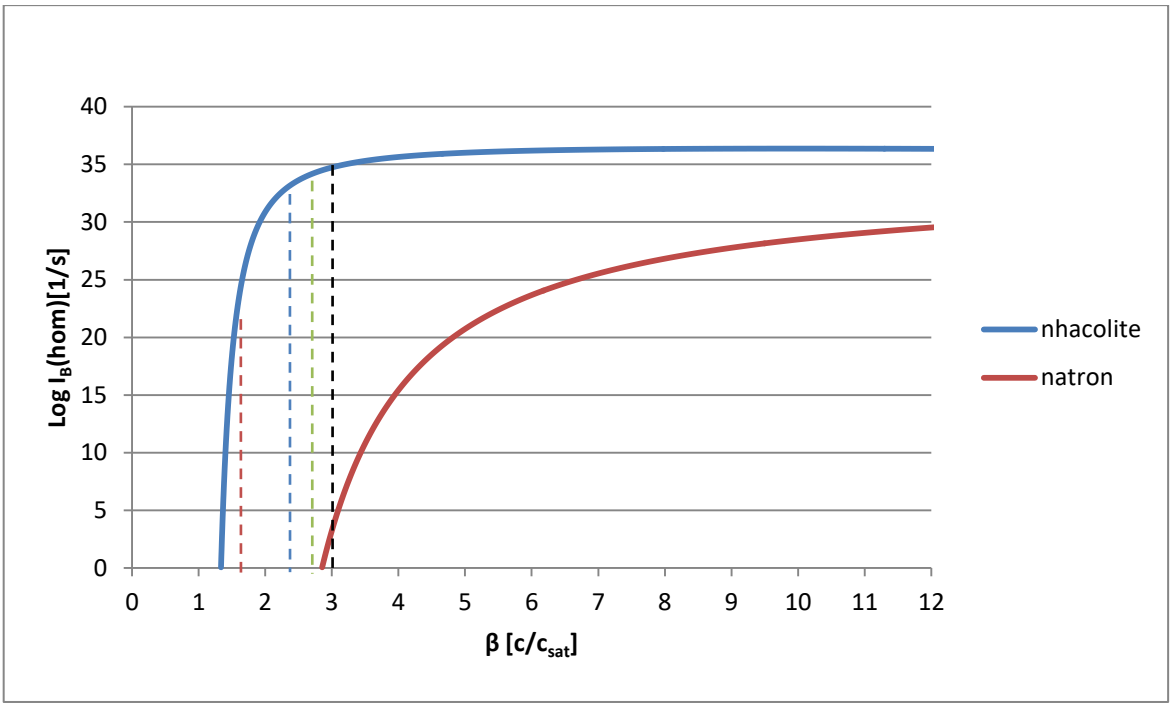

Fig. 32: Calculated nucleation density log(I_B) vs. supersaturation β (expressed as c/c_{sat}) for the homogeneous nucleation of nahcolite and natron according to Equation (6) (see section 1.3). Calculations performed using a value of Θ= 1 Rad (Espinosa-Marzal, personal communication), T=20°C selected from reference [100]. The molar volume was calculated from the density (nahcolite: 38.66 cm^3/mol, according to [100]; natron: 195.99 cm^3/mol, according to [101]). Dashed lines represent critical supersaturation values for: Control (red), CA 1 mM (blue), HEDP 1mM (green), PA 0.1 mM (black).

Solution	β [C/Csat]	LogI_B(hom) nahcolite [s^{-1}]	LogI_B(hom) natron [s^{-1}]
Control	1.52	17.67	0
Citrate 1mM	2.40	26.38	0
HEDP 1mM	2.80	27.08	0
PA 0.1 mM	2.88	34.53	0.65

Tab.7: Supersaturation indices and homogeneous nucleation density values reached by the four systems.

These calculated results show that nahcolite crystallizes earlier (i.e., at a lower supersaturation) than natron, confirming the evaluations carried out with PHREEQC.

Moreover results show that the control system crystallizes with a lower nucleation density than the other systems where organic additives are present. This confirms their inhibitory effect on the nucleation of nahcolite, which therefore begins to nucleate at higher supersaturation values. It is interesting to note that both curves increase up to a certain degree of supersturation, then tend to stabilize, especially that of nahcolite. This is due to increased viscosity of the system that reduces the mobility of ions and acts as an obstacle to nucleation, thereby strongly affecting the nucleation density [99].

With DLS it was possible to disclose that these inhibitors, used at a concentration lower than the one that totally inhibit the nucleation of nahcolite, had an effect not only on nucleation but also on crystal growth of both nahcolite and natron.

The radius of particles obtained through DLS were plotted with respect to time (Figure 33) in order to analyze how the systems evolved.

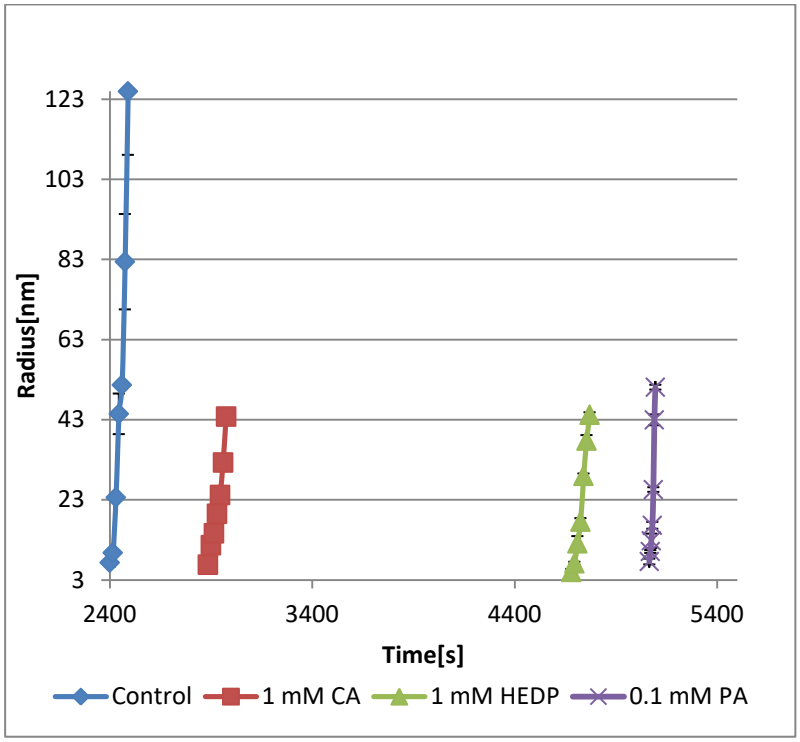

Fig. 33: Particle radius vs. time for the homogeneous nucleation of sodium bicarbonate in the absence (control) and in the presence of additives. Plotted values were obtained during the first 105 seconds from the beginning of the PSD analysis. Values are average of three replicates; error bars indicate standard deviation.

In general, it is possible to notice that all tested inhibitors delayed the formation of nahcolite (and natron) particles and reduced their dimensions. In other words, the additives had an effect both in the nucleation process and in the growth of the particles.

The explanation for the reduction of particle dimensions may be that, in the presence of an inhibitor, the system stabilizes with a consequent increase in the surface energy of crystal particles [53; 102].

Since the surface energy corresponds to the work that needs to be done to increase by one unit the crystal surface area, if it increases, spontaneous growth via monomer-by-monomer incorporation into the crystal lattice [103] will be disadvantageous [102].

By increasing the surface energy, the additives may affect not only the size but also the morphology of crystal particles. This is so because the morphology of a crystal is determined by the slowest growing faces as a consequence of the relative growth rates of the various faces of the crystal [35]. The growth rates of the different faces are influenced by external factors such as impurities, temperature and the choice of solvents. The change of morphology due to the effect of additives with respect to the Control solution is developed in section 3.5.

3.4 Macroscale salt crystallization tests and pore size distribution

Thanks to the accelerated aging of stone samples in the climatic chamber (see section 2.5), it was possible to test the effect of the selected organic inhibitors at the macroscale.

After 30 days aging, as shown in Figure 34, all stone samples had superficial pores occluded and an increased surface roughness. However, there was no visible difference to the naked eye among them.
The Control samples did not show great damage. This might be due to the fact that the temperature and RH conditions imposed in the climatic chamber led to the precipitation of sodium carbonate in the more and in the less hydrated forms (natron, thermonatrite, nahcolite, see section 1.2 Figure 4a). Considering that the first precipitated phase is nahcolite, what would happen is that the less hydrated forms did not cause damage to the stone material following dissolution and re-precipitation cycles, unlike natron which, as seen in other studies (Encarnacion Ruiz-Agudo personal communication), led quickly to considerable material degradation following dissolution-re-precipitation cycles involving the formation of less and more hydrated phases.

The percentage change in weight of the samples showed an interesting result. As shown in table 8, once the test in the climatic chamber was completed, all the specimens lost weight. This is because stone blocks were cyclically immersed in saturated bicarbonate solutions with and without additives for 30 days, 4 hours a day (see section 2.5). Actually, during the immersion period two phenomena can happen: soluble salts present in the samples leave the material and the water alters the stone by causing its disintegration (in our case material residues were found on the bottom of the crystallizer). Both phenomena cause weight loss of the material.

Solution	Control	CA 10 mM	PA 1 mM	HEDP 10 mM
% Weight loss	-0.19	-4.36	-4.05	-4.18

Tab. 8: Stone samples % weight loss after the treatment in the climatic chamber.

The stone samples with the lowest weight decrease were the ones immersed in the Control solution. This may mean that these three samples have balanced the weight loss due to the loss of soluble salt and water degradation by introducing into the structure

sodium and bicarbonate ions which increased the stone weight by precipitating as sodium (bi)carbonate crystalline forms. On the contrary, samples treated with solutions containing the inhibitors lost more weight. This may be due to the fact that the inhibitors have partially shielded the cations in solution, preventing their incorporation into the stone. Therefore, the greater weight loss of the samples treated with organic additives could be attributed to the loss of soluble salts from the samples and their alteration caused by water.

It must be specify that all the samples contain salts prior to testing and that the initial weight of all samples was determined without eliminating these salts naturally present in the material.

So, the lower weight loss of the samples treated in the Control solution could be due also to a lower initial content of soluble salts with respect to the samples treated in the solution containing the inhibitors. Because of this, all the statements made before about the weight loss are just hypothesis that could be confirmed by further analysis.

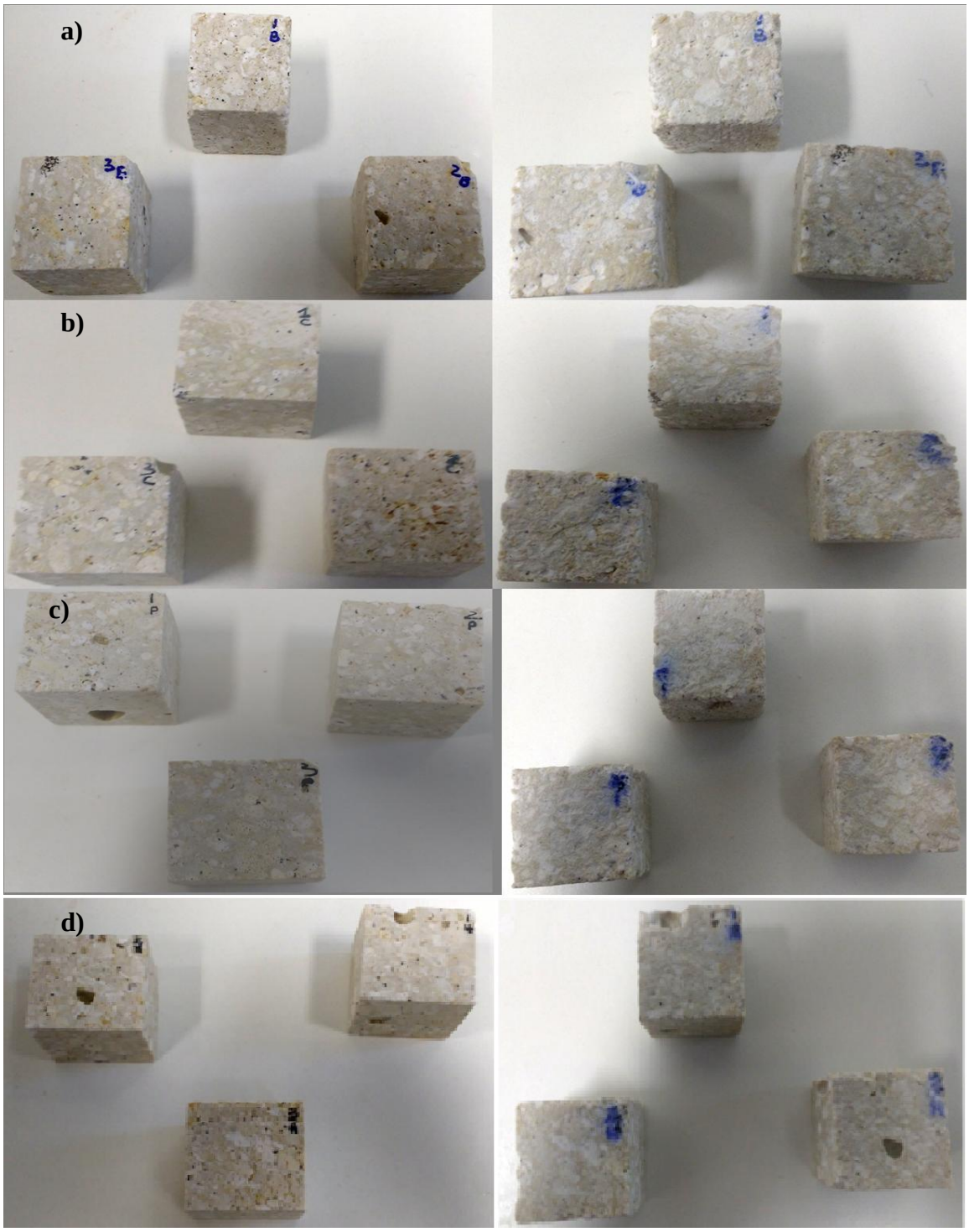

Fig. 34: On the left, stone samples before the treatment in the climatic chamber, on the right stone samples after 30 days of treatment. Solutions used. **a)** Control, **b)** 10 mM CA, **c)** 1mM PA, **d)** 10 mM HEDP.

A better picture of the macroscale effects of tested inhibitors is provided by mercury intrusion porosimetry tests (see section 2.5) performed on washed and not washed samples (Figure 35).

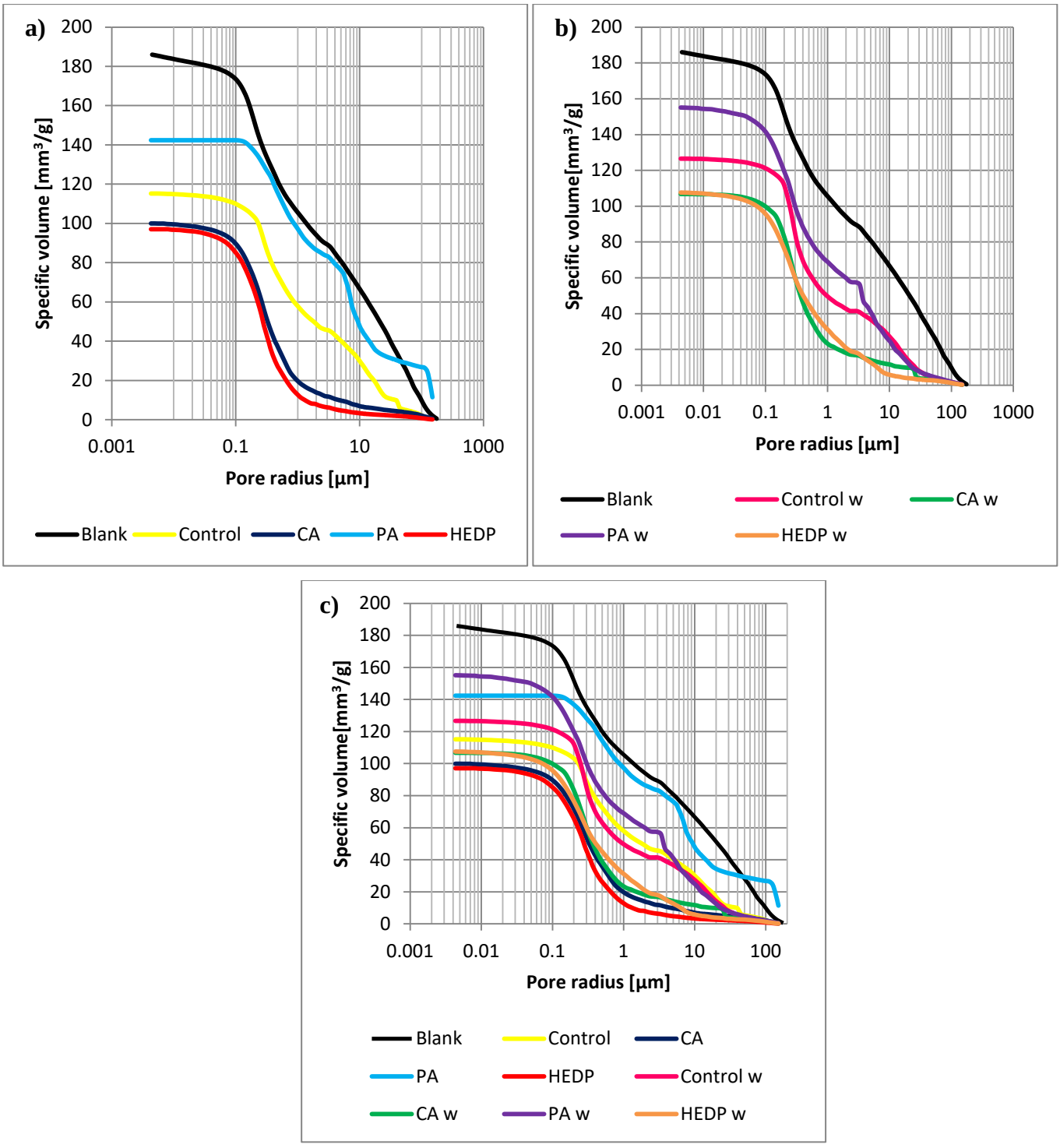

Fig. 35: Pore size distribution of samples treatment in the climatic chamber, not washed (a) and washed (b). Graph (c) is the overlapping of (a) and (b). *Blank* denoted untreated samples.

As shown in Figure 35a, 1mM PA seems to be the most effective inhibitor because the volume of mercury penetrated into free pores is almost comparable to the *Blank*. This means that the open porosity of the untreated material is comparable to that of the

material exposed for 30 days to the climatic chamber treatment in a solution containing PA. In other words, by preventing the crystallization of sodium carbonate-bicarbonate crystals within the stone pores, only efflorescence formed in these experiment. This means that no damage to the stone substrate would occur in the presence of PA.

As for the samples treated with 10 mM CA and 10 mM HEDP, it seems that they decreased the percentage of open porosity of the material. This may be due to the fact that the crystals generated in the solutions containing such inhibitors have smaller dimensions than the ones in the control solution, an explanation perfectly supported by the results obtained with DLS (see section 3.3 Figure 33). Thus, the formation of smaller crystals might lead to the occlusion of the smaller pores of the stone material. To provide a better explanation for that, logarithmic differential pore volume distribution vs. pore radius was plotted (Figure 36).

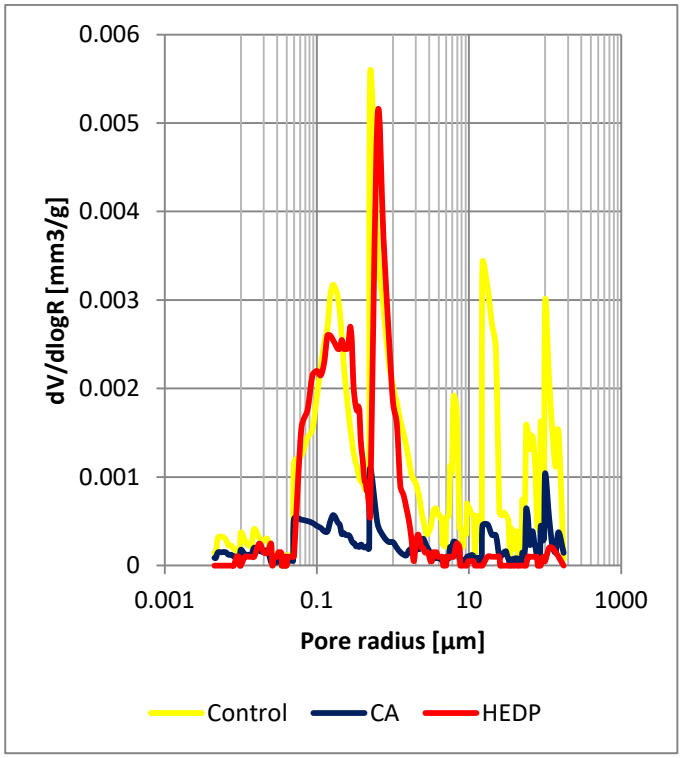

Fig. 36: Pore size distribution of not washed samples treated in a climatic chamber.

Logarithmic differential pore volume distribution shows which pore volume can be ascribed to which pore size. As shown in figure 36, the curves of the CA and HEDP are below the Control curve. This could mean that the stone pores are better filled from crystals formed in the CA and HEDP solutions.

As regards washed samples, in Figure 35b-c it is shown that after the treatment in water the trends remained unaltered but the open porosity increased. This happened because washing the samples causes the dissolution of the soluble salts that are on the stone surface and in the bulk, which are then removed from the material by water action.

It must be noticed that the *Blank* is much more porous than the rest of the stones: even after all salts have been eliminated, the total intruded volume is systematically higher in the *Blank* than in the rest of the samples. This just shows that the stone samples were highly heterogeneous, with significant changes in porosity among them, which makes it very hard to reach any satisfactory conclusion about the outcome of these tests.

That's why for a more complete picture of crystallization of sodium carbonate-bicarbonate within the calcareous rock porosity, the results obtained in this section are further developed and discussed in the following section.

3.5 FESEM observations

The analysis with FESEM allowed us to observe the morphology with which nahcolite, natron and thermonatrite precipitated with and without a support (see section 2.6).

In order to visualize the change in morphology due to the effect of additives with respect to the control solution, a small aliquot of precipitate of each solution (Control, CA 1 mM, PA 0.1 mM, HEDP 1 mM) was taken at the end of the crystallization tests in solution and subsequently dried in an oven at 55°C. FESEM photomicrographs of the collected solids are shown in Figure 37.

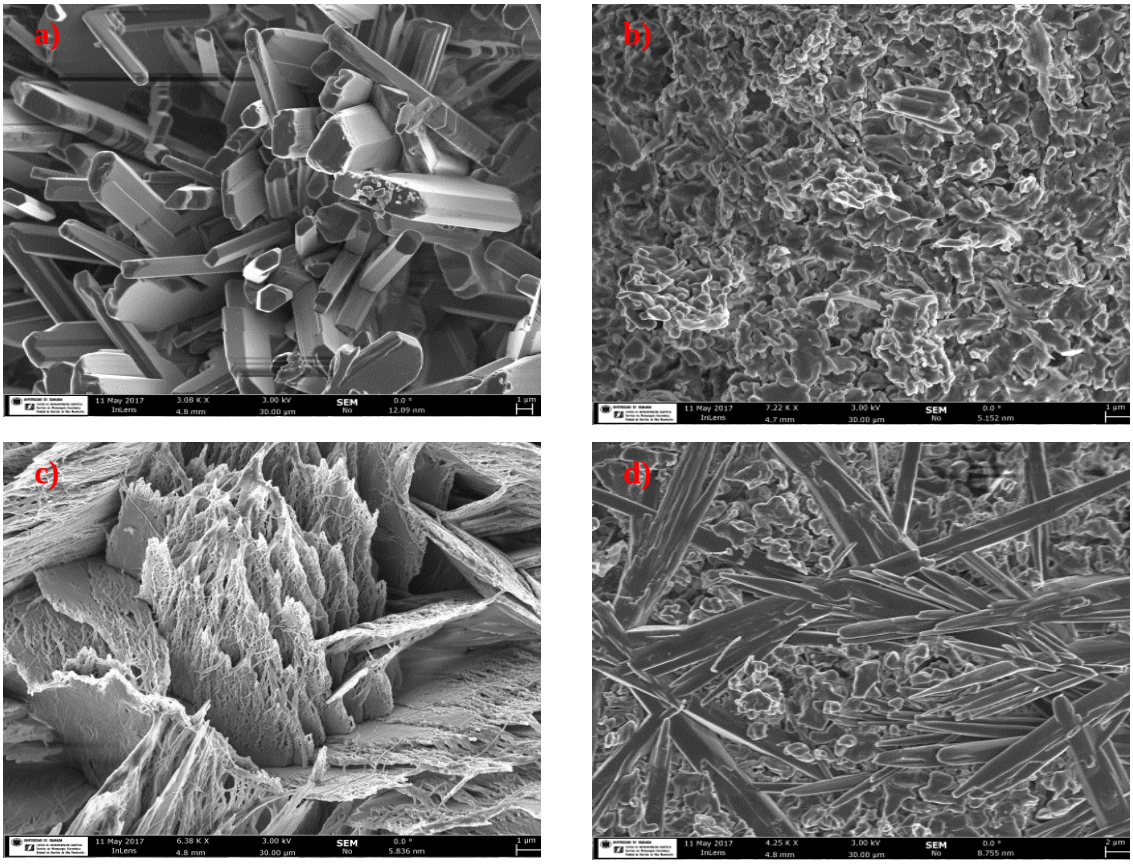

Fig. 37: FESEM photomicrographs of sodium bicarbonate crystals formed during homogeneous crystallization in (a) a pure sodium bicarbonate solution (Control), and in the presence of (b) 1 mM CA, (c) 0.1 mM PA, (d) 1 mM HEDP.

Nahcolite crystals show a prismatic shape that changed according to the inhibitor used. Moreover the additives significantly reduced the crystals size, in agreement with DLS results (see section 3.3, Figure 33).

In Figure 37b it can be noticed that CA seems to act in a nonspecific manner, by adsorbing on all the faces of the crystal. However, some elongated structures have also been found in the sample, as shown in Figure 38a. The formation of the elongated structures is due to the fact that the morphology of a growing crystal is determined by the relative growth rates of its faces [35; 104]. The faster the growth rate in the direction perpendicular to a particular face, the smaller that face forms. According to Ruiz-Agudo et al. [6] DTPMP has the same effect on epsomite crystals when dosed at a concentration of 10 mM as that observed here for the case of nahcolite formed in the presence of CA. DTPMP in fact led to an habit change that could be interpreted through preferential additive adsorption on epsomite {110} faces and, to a lesser extent, on {020} faces. The growth of these faces was thus slowed down, resulting in the overdevelopment of the {110} form along the c-axis that changed the crystals' habit from prismatic to acicular (a schematic representation of that effect is shown in Figure 39). The same mechanism could be applied to nahcolite crystals.

PA generated rather jagged structures which, as can be seen in Figure 38b, would seem to consist of bundles of multiple fibres.

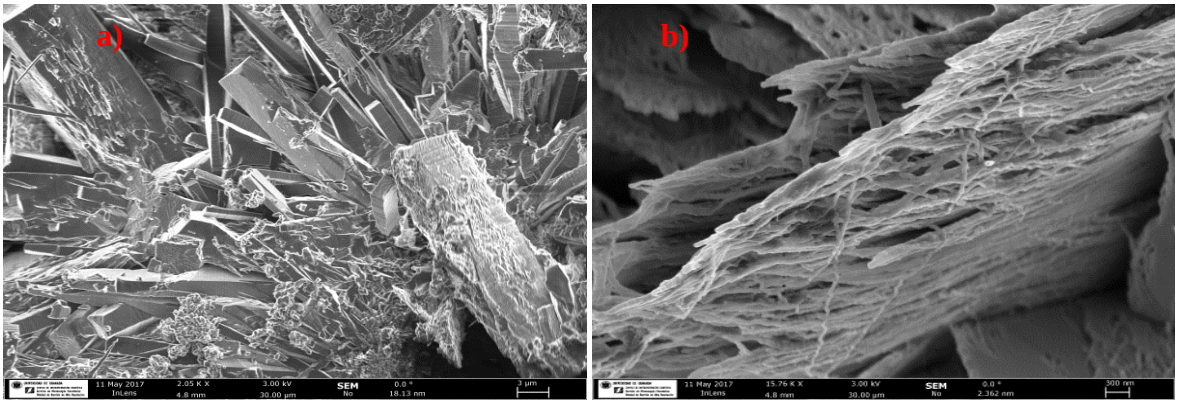

Fig. 38: Detailed FESEM photomicrographs of nahcolite crystals grown in the presence of (a) 10 mM CA and (b) 0.1 mM PA.

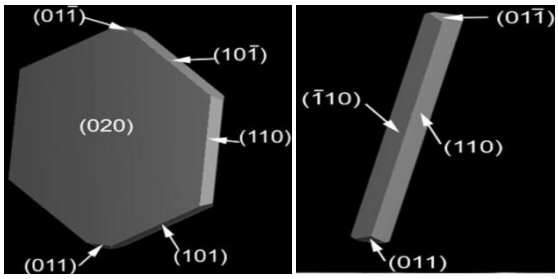

Fig. 39: Schematic representation of the change in habit of epsomite crystals when grown in the absence (on the left) and in the presence (on the right) of DTPMP dosed at a concentration of 10 mM [6].

From Figure 37 it is also possible to notice that HEDP led to the formation of structures similar to those seen for CA but, unlike CA, the elongate structures were more widespread.

Overall, the photomicrographs in Figure 37 show that the crystal density in the presence of CA, PA and HEDP was much higher than in the control.
This can be due to the higher nucleation density reached (i.e. higher supersaturation) in the presence of the additives (see section 3.3, Fig. 32), which substantially increases the number of smaller crystals [35], in full agreement with our nucleation density calculations.
FESEM analyses were also carried out on a drop of solution, with and without additives, placed on a calcite support and let to crystallize by evaporation (see section 2.6). This experiment was done in order to determine if there was a preferred crystallographic orientation induced by the substrate, that is, the Iceland spar (10.4) rhombohedral face, which is the most common face of calcite. The latter would demonstrate that calcite crystals in the stone (calcarenite) could act as heterogeneous nuclei, favouring the crystallization of sodium (bi)carbonate at a relatively low supersaturation (i.e., minimal damage). The experiment also strived to disclose the effect that the additives adsorbed onto calcite had on the nucleation of the salts. As shown in Figure 40a, nahcolite crystals grown on the calcite support in the absence of additives displayed a palm-tree/feather-like shape consisting of a coalescence of fibres. According to the literature[105], the fibrous aspect is the typical one found in nature for nahcolite. The observations made towards the edge of the sample allowed to detect the presence of larger clusters, always consisting of smaller fibrous clusters. The latter could be thermonatrite crystals as the morphology observed is in agreement with that reported in the literature [105; 106]. These observations show that the substrate exerted no crystallographic control on the crystallization of sodium carbonate-bicarbonate phases.

In Figure 40b it can be seen that in the presence of CA the crystal shape changed. CA presence led to the formation of elongated structures that were always made of bundles of fibres.

Crystals formed in the presence of PA and HEDP showed similar structures, referable to those found on the edge of the sample containing the Control solution (Figure 40c and d). The fact that the salt crystals developed on the calcite substrate in the presence of additives displayed no preferred orientation, confirmed that calcite does not facilitate the heterogeneous nucleation of sodium carbonate phases irrespectively of the absence or presence of additives.

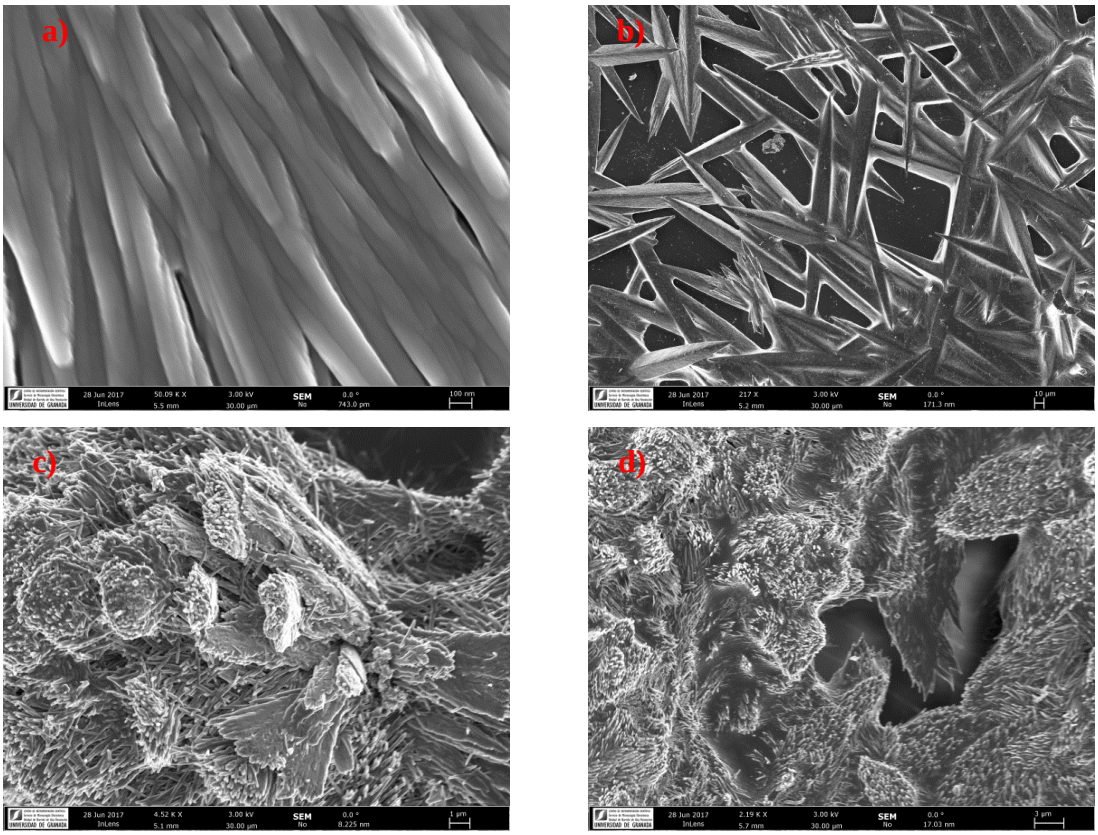

Fig. 40: FESEM photomicrographs of sodium bicarbonate crystals formed by evaporation on a calcite crystal of (a) a pure sodium bicarbonate solution (Control), and in the presence of (b) 10 mM CA, (c) 1 mM PA, (d) 10 mM HEDP.

FESEM analyses were also carried out on stone materials (limestone from Santa Pudia) after treatment in the climatic chamber (see section 2.5), with and without additives, in order to determine how crystallization happens in a porous media. The photomicrographs obtained are shown in Figure 41.

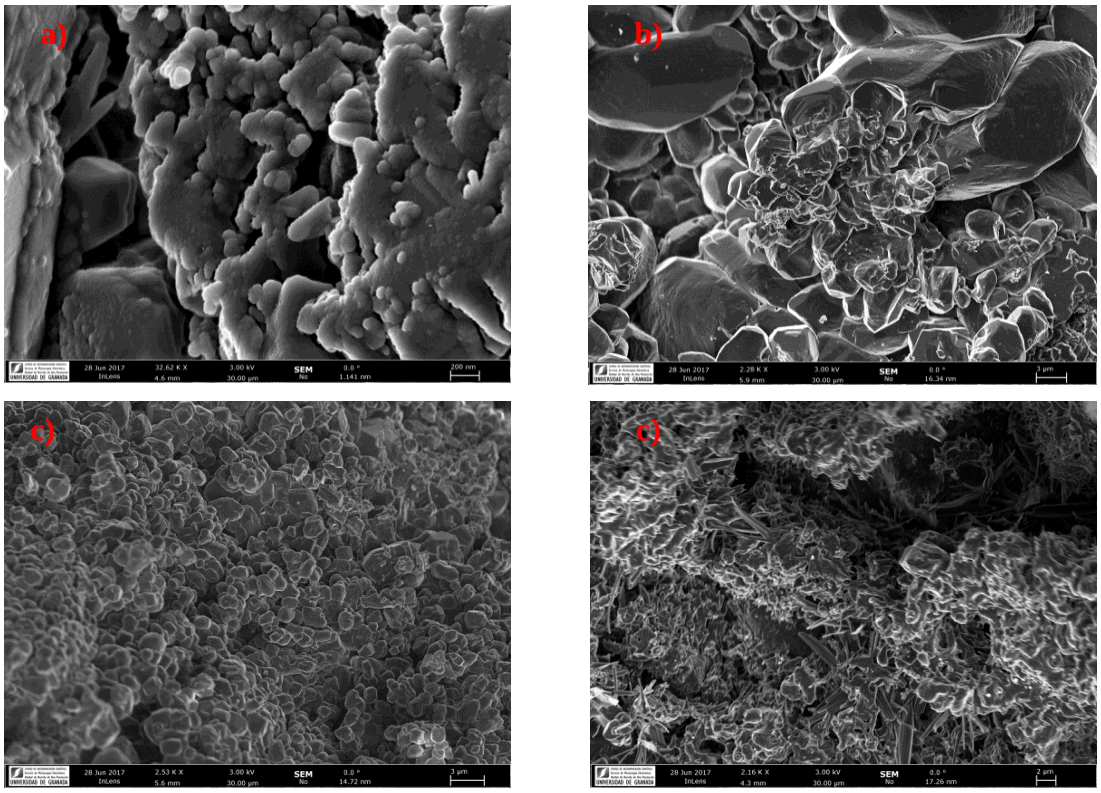

Fig. 41: FESEM photomicrographs of sodium bicarbonate crystals formed within a limestone from Santa Pudia quarry of (a) a pure sodium bicarbonate solution (Control), and in the presence of (b) 10 mM CA, (c) 1 mM PA, (d) 10 mM HEDP.

As shown in Figure 41a, nahcolite crystals crystallize in the open porosity with an acicular habit.

As for CA, it would seem that nahcolite is not present in the sample. This may be explained by the fact that crystallization probably occurred more in the form of efflorescence than subflorescence and therefore it was not possible to observe the presence of salts within the material.

However, this result is not consistent with the results obtained by mercury intrusion porosimetry (see section 3.4, Figure 35a-36), which showed a decrease in open porosity in the presence of CA, probably due to the reduction of the crystal size caused by the inhibitor that facilitated the filling of the smallest pores in the stone.

A further explanation might be that nahcolite may have crystallized as shown in Figure 37b, so that the crystals may have assumed a shape similar to that of the calcite crystals in the calcarenite, being difficult to distinguish them.

Even for PA it would seem that no nahcolite was present in the sample. However, unlike CA, the fact that crystallization could have taken place more in the form of efflorescence than subflorescence is supported by the result obtained by mercury intrusion porosimetry

(see section 3.4, Figure 35a), which showed an increased open porosity compared to the sample treated with the control solution.

As for HEDP, the photomicrograph in Figure 41d shows widespread acicular structures within the stone material.

This result is in perfect agreement with those obtained through mercury intrusion porosimetry, that is, a reduction in open porosity, associated with the filling/clogging of the smallest pores, likely caused by the reduction in the size of the crystals.

4. Conclusions

In this work a number of phosponate and carboxylate additives were tested as potential crystallization modifiers for sodium carbonate- bicarbonate crystallization: sodium citrate tribasic dihydrate (CA), L-aspartic acid sodium salt monohydrate (AAS), polyacrylic acid 2100MW (PA), etidronic acid (HEDP), aminotris(methylenephosphonic) acid (ATMP) and diethylenetriaminepentakis-(methylphosphonic) acid (DTPMP).

Phases precipitated during crystallization in bulk solution (following a *T* drop) and evaporation tests, identified using XRD, were nahcolite ($NaHCO_3$), natron ($Na_2CO_3 \cdot 10H_2O$) and thermonatrite ($Na_2CO_3 \cdot H_2O$). Natron and thermonatrite only formed in bulk solution and evaporative crystallization tests, respectively. XRD results in combination with modelling using the thermodynamic code PHREEQC and the calculation of the nucleation rate demonstrated that nahcolite was the first phase formed during both tests. The formation of the other phases may depend on the experimental conditions in which the two tests were conducted.

Considering the different additives tested, several act as inhibitors of nahcolite crystallization and growth, while others do not show significant effects. Electrostatic interactions between the deprotonated functional groups of organic additives and the cations in solution or in pre-nucleation clusters and/or embryos (with size below the critical size) appears to be the principal mechanism of additive-nahcolite interaction at the pre-nucleation stage.

Small molecules with low charge, such as AAS, and large branched molecules with several functional groups (ATMP, DTPMP) do not have any significant effect, whereas highly deprotonated small molecules (CA, HEDP) and macromolecules (PA) inhibit the nucleation of nahcolite during crystallization tests in solution.

This could be attributed to the fact that the large and branched molecules display poorer adsorption on the surface of the crystallization embryos, which then aggregate and form the final macroscopic sodium bicarbonate crystals.

Studying the variation of nucleation density and crystal growth with and without the additives it was possible to notice that during the crystallization tests from solution, the tested inhibitors delay the formation of nahcolite , and consequently natron particles, and reduce their dimensions. In other words, the additives have an effect both in the nucleation process and in the growth of the particles.

Stabilization of the system as a consequence of the increasing particle surface energy suggested by Ragavan et al. [53] and Osazaki et al.[102] appears to be the explanation for both phenomena.

Salt weathering tests, in addition to mercury intrusion porosimetry tests (MIP) allowed us to quantify the damage induced by such salts as well as the effect the additives have on the in pore crystallization of sodium carbonate phases and associated damage.

After 30 days of salt weathering cycles, all stone samples have superficial pores occluded by salts and an increased surface roughness. Control samples did not show great damage. This may be due to the fact that the temperature and RH conditions imposed in the climatic chamber led to the precipitation of sodium carbonate in the more and in the less hydrated forms (natron, thermonatrite, nahcolite). Considering that the phase that precipitates as first and in greater quantities is nahcolite, what would happen is that less hydrated forms do not cause damage to the stone material by subsequent dissolution and re-precipitation, unlike natron which, as seen in other studies (Encarnacion Ruiz-Agudo personal communication), led quickly to considerable material degradation.

MIP confirms that PA was the most effective inhibitor because the volume of mercury penetrated into free pores is almost comparable to the Blank. This means that the open porosity of the material untreated in the climatic chamber is comparable to that of the material exposed for 30 days to the climatic chamber treatment in a solution containing $NaHCO_3$ 12% w/w and 1mM PA. The latter implies that almost all salts present in the saline solution saturating the stone were induced to crystallize as efflorescence. This occurs because during drying, the additive (PA) strongly inhibits in pore salt crystallization, thereby enabling the solution to reach the stone surface and evaporate there before crystallization occurs. Formation of non-damaging effloresce prevents salt damage to develop in the calcarenite.

As for the samples treated with CA and HEDP, it seems that these additives induce a decrease in the open porosity of the material. This may be due to the fact that the crystals generated in the solutions containing such inhibitors precipitate as very small crystals which fill the small pores in the calcarenite. Formation of crystals smaller than those precipitated in the absence of these additives is consistent with the results obtained with the DLS and FESEM.

FESEM observation allowed us to understand that the inhibitors led to a change in the morphology of the precipitated crystals, resulting in thin and elongated prisms in the case of CA and HEDP or forming fibrous bundles in the case of PA.

From the obtained results, it is clear that 10 mM CA, 10 mM HEDP and 1 mM PA inhibited the formation of nahcolite and reduced the damage caused by its crystallization. Our results also show that 1 mM PA seems to be the most effective inhibitor.

The use of such promising crystallization inhibitors could lead to the development of more efficient treatments for preventive conservation of ornamental stone affected by crystallization damage due to the different crystalline forms of sodium carbonate and bicarbonate.

References

[1] Steiger, M., Asmussen, S. (2008): Crystallization of sodium sulfate phases in porous materials: the phase diagram Na_2SO_4–H_2O and the generation of stress. *Geochimica et Cosmochimica Acta* 72, pp. 4291-4306.

[2] Rodriguez-Navarro C., Doehne E., Sebastian E. (2000): How does sodium sulfate crystallize? Implications for the decay and testing of building materials. *Cement and Concrete Research* 30, pp. 1527- 1534.

[3] Selwitz C., Doehn E. (2002): The evaluation of crystallization modifiers for controlling salt damage to limestone. *Journal of Cultural Heritage* 3, pp. 205-216.

[4] Rodriguez-Navarro C., Linares-Fernandez L., Doehne E., Sebastian E. (2002): Effects of ferrocyanide ions on NaCl crystallization in porous stone. *Journal of Crystal Growth* 243, pp. 503–516.

[5] Ruiz-Agudo E., Rodriguez-Navarro C., Sebastian Pardo E. (2006): Sodium Sulfate Crystallization in the Presence of Phosphonates: Implications in Ornamental Stone Conservation. *Crystal Growth & Design* 6, pp. 1575- 1583.

[6] Ruiz-Agudo E., V. Putnis C., Rodriguez-Navarro C., (2008):Interaction between Epsomite Crystals and Organic Additives. *Crystal Growth & Design*, 8, pp. 2665-2673.

[7] Rodriguez-Navarro C., G. Benning L., (2013): Control of Crystal nucleation and growth by organic additives. *Elements*, 9, pp. 203–209.

[8] Nancollas, G.H. (1984): inhibitors of crystallization and dissolution. *Industrial Crystallization* 84, pp. 51-59.

[9] Gebauer D., Cölfen H., Verch A., Antonietti M. (2009): The multiple roles of additives in $CaCO_3$ crystallization: A quantitative case study. *Advanced Materials* 21, pp. 435–439.

[10] Tantayakom, V., Fogler, H.S., Charoensirithavorn, P., Chavadej, S. (2005): Kinetic study of scale inhibitor precipitation in squeeze. *Crystal Growth & Design*, 5, pp. 329-335.

[11] Espinosa-Marzal R., Hamilton A., Mc Nall M., Whitaker K.(2011): The chemomechanics of crystallization during rewetting of limestone impregnated with sodium sulfate. *Journal of Material Research*, 26, pp. 1472-1481.

[12] Schiro M., Ruiz-Agudo E., Rodriguez-Navarro C. (2012): Damage Mechanisms of Porous Materials due to In-Pore Salt Crystallization. *Physical Review Letters* 109, 265503.

[13] Rodriguez-Navarro C., Linares-Fernandez L., Doehne E., Sebastian E. (2002): Effects of ferrocyanide ions on NaCl crystallization in porous stone. *Journal of Crystal Growth* 243, pp. 503-516

[14] Goudie A., Viles H., (1997): *Salt Weathering Hazards*. John Wiley & Sons, pp. 237.

[15] Benavente D., Brimblecombe P., Grossi C.M. (2015): Thermodynamic calculations for the salt crystallisation damage in porous built heritage using PHREEQc . *Environmental Earth Sciences* 74, pp. 2297–2313.

[16] Helvaci C., Dokuz E., (1998): The Beypazari trona deposit, Ankara Province, Turkey. Wyoming State Geological Survey Public Information Circular 40.

[17] Zehender K., Arnold A. (1989): Crystal growth in salt efflorescence. *Journal of Crystal Growth*, 97, pp. 513-521.

[18] P. Gasparoli (2002): *Le superfici esterne degli edifici*: *degradi, criteri di progetto, tecniche di manutenzione*, Alinea Editrice.
[19] L. Backbier, J. Rousseau (1993): Analytical study of salt migration and efflorescence in a medieval cathedral. *Analytica Chimica Acta*, 283, pp. 855-867.
[20] Rodriguez-Navarro C., Doehne E., Ginell W., (1996): Salt growth in capillary and porous media. Libro de comunicaciones del III Congreso Internacional de Rehabilitaciòn del Patrimonio Arquitectónico y Edificación; Sebastian Pardo E., Valverde Espinosa I., Zezza U. (Eds.), Granada, pp. 509-514.
[21] Soragni E., Gualtieri S., Samperisi L., Bernardi E. (2016): Geopolymers: Innovative Materials for Conservation Works. Proceedings of the 5th International Conference Youth in Conservation of Cultural Heritage – YOCOCU 2016, 21-23 September 2016, Madrid, Spain. (in press).
[22] D.Camuffo (1995): The physical weathering of stones. *The Science of the Total Environment* 167, 1-14
[23] Flatt, R. J. (2002): Salt damage in porous materials: how high supersaturations are generated. *Journal of Crystal Growth* 242, 435-454.
[24] Flatt, R. J., Scherer, G. W. & Steiger, M. A (2007): Commented translation of the paper by C.W. Correns and W. Steinborn on crystallization pressure. *Environmental Geology* 52, 187–203.
[25] Arnold A., Kueng A., (1985): Crystallization and habits of salt efflorescences on wall. Methods of investigation and habits. V congrès international sur l'alteration et la conservation de la pierre. Actes. Proceedings, Lausanne, 25-27-9, Presses polytechniques romandes, pp. 269-277.
[26] Fahey, J.J., Yorks K.P. (1963): Wegscheiderite (Na_2CO_3•3NaHCO3), a new saline mineral from the Green River Formation, Wyoming. *American Mineralogist*, 48, 400–403;
[27] www.mineraldata.it; access 19/06/2017, time: 13.52.
[28] Material supplied by Ruiz-Agudo E.
[29] Monnin C., Schott J. (1983): Determination of the solubility products of sodium carbonate minerals and an application to trona deposition in Lake Magadi (Kenya). *Geochimica et Cosmochimica Acta*, 48. 571-581.
[30] Winkler E. M., Wilhelm E. J. (1970): Saltburst by hydration pressures in architectural stone in urban atmosphere. *Geological Society of America Bulletin* 81, 567-572.
[31] Sperling C. H. B., Cooke R.U (1985): Laboratory simulation of rock weathering by salt crystallization and hydration processes in hot, arid environments. *Earth Surf Processes Landforms*, 10, pp.541-555.
[32] Fahey B.D (1986): A comparative laboratory study of salt crystallization an salt hydration as potential weathering agents in deserts, *Geografiska Annaler. Series A. Physical Geography*,68, pp. 107-111.
[33] Flatt R.J (2002): Salt damage in porous materials: how high supersaturations are generated. *Journal of Crystal Growth*, 242, pp. 435-454.
[34] Mortensen H. (1933): Die "Salzprengung" und ihre Bedeutung für die regional klimatische Gliederung der Wüsten. *Petermanns Geographische Mitteilungen* 79, 130-135.
[35] Mullin J.W. (2001): *Crystallization*, 4th edition. Butterworth Heinemann, Oxford.
[36] Porter, D. A., Easterling, K. E. (1992). Crystal Interfaces and Microstructure (Chapter 3). In *Phase Transformations in Metals and Alloys*, second edition, USA, Taylor and Francis group, pp. 110-184.

[37] De Yoreo J.J, Vekilov P.G (2003): Principles of crystal nucleation and growth. *Reviews in Mineralogy & Geochemistry*, Vol.3 chapter 3, 57-92.
[38] Correns, C. W., & Steinborn, W. (1939): Experimente zur Messung und Erklärung der sogenannten Kristallisationskraft. *Zeitschrift für Kristallographie - Crystalline Materials* 01, 117–135.
[39] Söhnel O. (1981): Electrolyte crystal-aqueous solution interfacial tensions from crystallization data. *Journal of Crystal Growth* 57, 101-108.
[40] Gibbs, J. W.(1876): On the equilibrium of heterogeneous substances. *Transaction of the Connecticut Academy of Arts and Sciences* 3, 108–248.
[41] Gibbs, J.W. (1878): On the equilibrium of heterogeneous substances. *Transaction of the Connecticut Academy of Arts and Sciences* 16, 343–524.
[42] Gebauer, D., Kellermeier, M., Gale, J.D., Bergström, L., Cölfen, H. (2014) Pre-nucleation clusters as solute precursors in crystallization. *Chemical Society Reviews* 43, 2348-2371.
[43] Nielsen, A. E. & Toft, J. M. (1984): Electrolyte crystal growth kinetics. *Journal of Crystal Growth* 67, 278-288.
[44] Nancollas H.G. (1979): The growth of crystals in solution. *Advances in Colloid and Interface Science*, 10, 215-252.
[45] Kossel, W. (1927): Zur Theorie des Kristallwachstums. *Nachrichten von der Gesellschaft der Wissenschaften zu Göttingen, Math-Phys. Klasse*, 135-143.
[46] Meldrum, F., Cölfen, H. (2008): Controlling mineral morphologies and structures in biological and synthetic systems. *Chemical Reviews* 108, 4332- 4432 .
[47] Black S.N, Bromely L.A, Cottier D., Davey R.J., Dobbs B., Rout J.E. (1991): Interaction at the organic/inorganic interface: binding motifs for phosphonates at the surface of barite crystals. *Journal of the Chemical Society, Faraday Transactions*, 87, 3409-3414.
[48] Bosbach D., Coveney P.V., Griffin J. L. W., Putnis A., Risthaus P., Stackhouse S., Whiting A. (2002): The rational design, synthesis and demonstration of the recognition and binding of a diaza-dioxa-12-cown-4 diphosphonate macrocycle to all crystal growth faces of barium sulphate. *Journal of the Chemical society, Perkin Transactions*, 2, 1238-1245.
[49] Garcia C., Courbin G., Ropital F., Fiaud C. (2001): Study of the scale inhibition by HEDP in a channel flow cell using a quartz crystal microbalance. *Electrochimica Acta*, 46, 973- 985.
[50] Bishop M., Bott S.G., Barron A. R(2003): A new mechanism for cement hydration inhibition: solid state chemistry of calcium notrolotris(methylene)triphosphonate. *Chemistry of Materials*, 15(16), 3074-3088.
[51] Lanzón M., García-Ruiz P.A (2012): Effect of citric acid on setting inhibition and mechanical properties of gypsum building plasters. *Construction and Building Materials* 28, 506–511.
[52] Taylor L.S, Zografi G. (1997): Spectroscopic caraterization of interactions between PVP and Indomethacin in amorphous molecular dispersion. *Pharmaceutical Research* 14, 1691-1698.
[53] Raghavan, S.L., Trividic, A., Davis, A.F., Hadgraft J. (2001): Crystallization of hydrocortisone acetate: influence of polymers. *International Journal of Pharmaceutics* 212, 213–221.
[54] Davey, R. J. Mullin J.W. (1974): Growth of the {100} faces of ammonium dihydrogen phosphate crystals in the presence of ionic species. *Journal of Crystal Growth* 26, 45—51.

[55] Bennema P. (1969): The importance of surface diffusion for crystal growth from solution. *Journal of Crystal Growth* 5, 29-43.
[56] Larson M.A, Mullin J.W (1973): Crystallization kinetic of ammonium sulfate. *Journal of Crystal Growth* 20, 183-191.
[57] Sears G.W (1958): Effect of poisons on crystal growth. *Journal of Chemical Physics* 29. 1045.
[58] Burril K.A. (1972): A model of crystal growth rates under surface diffusion control in impure solution. *Journal of Crystal Growth* 239-244.
[59] Farmanesh S., Chung J., Sosa D.R., Ha Kwak J., Karande P., Rimer D. J. (2014): Natural promoters of calcium oxalate monohydrate crystallization. *Journal of the American Chemical Society*, 136, 12648−12657.
[60] Wang L., Nancollas G.H (2010): Dynamics of biomineralization and biodemineralization. *Metal Ions Life Science,* 4, 413–456.
[61] Liu X.Y., De Yoreo J.J (2004): *From Solid-Fluid Interface to Nanostructure Engineering.* II edition. Plenum/Kluwer; New York.
[62] Ralston P.H (1972): Inhibiting water formed deposits with threshold composition. *Materials Protection and Performance,* 11, 39-44.
[63] Lin J., Wu J., Yang Z., Pu M. (2001): Synthesis and properties of poly(acrylic acid)/mica superabsorbent nanocomposite. *Macromolecular Rapid Communication*, 22, 422–424.
[64] van Rosmalen G.M. (1983): Scale prevention with special reference to threshold treatment. *Chemical Engineering Communication*, 20, 209-233.
[65] Jonasson R.G., Rispler K., Wiwchar B., Gunter W. D. (1996): Effect of phosphonate inhibitors on calcite nucleation kinetics as a function of temperature using light scattering in an autoclave. *Chemical Geology*, 132, 215-225.
[66] Klepetsanis P.G, Koutsoukos P.G. (1998): Kinetics of calcium sulfate formation in aqueous media: effect of organophosphorus compounds. *Journal of Crystal Growth*, 193, 156-153.
[67] He S., Kan A.T. (1999): Inhibition of calcium carbonate precipitation in NaCl brines from 25°C to 90°C. *Applied Geochemistry*, 14, 17-25.
[68] Jones F., Oliveira A., Rohl A.L, Parkinson G.M, Ogden M.I., Reyhani M.M. (2002): Anomalous behaviour within a systematic series of barium sulphate growth modifiers. *Journal of Crystal Growth*, 237-239, 424-429.
[69] Badens E., Veesler S., Boistelle R. (1999): Crystallization of gypsum from hemihydrate in presence of additives. *Journal of Crystal Growth*, 198/199, 704-709.
[70] Reddy M.M, Hoch A.R (2001): Calcite crystal growth rate inhibition by polycarboxylic acids. *Journal of Colloid and Interface Science*, 235, 365-370.
[71] Stevenson T.D inventor and assignee: Process for making sodium bicarbonate from Nahcolite -rich solutions. United states patent US5588713A. 31/12/1996.
[72] Martin, J.; Alcantara, R.; Garcia-Ruiz J.M (1991): The detection of salting out. a comparative study. *Crystal Research and Technology*, 26, 35-42.
[73] Fabbri, B. Fiori, C. Ravaglioli A. (1989): *Materie prime ceramiche – Tecniche analitiche e indagini di laboratorio*, Biblioteca tecnica ceramica. Faenza Editrice. Ch. 8.
[74] Fifield F.W., Kealey D. (1999): *Chimica Analitica - teoria e Pratica*, 1st ed, Zanichelli, Bologna, Chapter 8.
[75] www.lsinstruments.ch.; access: 1/08/2017, time: 8.36 a.m.
[76] Berne, B.J., Pecora R. (2000): *Dynamic Light Scattering with Applications to Chemistry, Biology, and Physics*, Dover Publications, INC. Mineola, Ch 3.

[77] www.microtrac.com; access 1/08/2017, time: 10.02 a.m.
[78] Benavente D., García del Cura M.A., Bernabeu A., Ordoñez S. (2001) Quantification of salt weathering in porous stones using an experimental continuous partial immersion method. *Engineering Geology*. 59 [3–4], 313–325.
[79] Nicholson D.T. (2001) Pore properties as indicators of breakdown mechanisms in experimentally weathered limestones. *Earth Surface Processes and Landforms*. 26, 819–838.
[80] Chéné G., Bastian G., Brunjail C., Laurent J.P. (1999) Accelerating weathering of tuffeau block submitted to wetting–drying cycles. *Materials and Structures* 32, 525–532.
[81] Urosevic M., Pardo S.E., Ruiz-Agudo E., Cardell C. (2011): Evaluación de las propiedades físicas de dos rocas carbonáticas usadas como material de construcción actual e histórico en Andalucía Oriental, España. *Materiales de Construcción*, 61, 93-114.
[82] Olmedo J.G., Gomez Moreno J.M. (1986): *Arte y deterioro en los monumentos granadinos: catedral, chancillería y palacio de Carlos V*. Universidad de Granada, Junta de Andalucía, España.
[83] Youh Kuua W., Chilamkurtia Chi Chenb R. (1998): Effect of relative humidity and temperature on moisture sorption and stability of sodium bicarbonate powder. *International Journal of Pharmaceutics*, 166, pp. 167-175.
[84] BS ISO 15901-1:2016: Evaluation of pore size distribution and porosity of solid materials by mercury porosimetry and gas adsorption. Part 1: Mercury porosimetry.
[85] Ritter H.L., Drake L.C. (1945): Pore size distribution in porous materials. I. Pressure porosimeter and determination of complete macropore size distributions. *Industrial & Engineering Chemistry Analytical Edition*, 17, 782–786.
[86] www.micromeritics.com; access 3/08/2017, time: 8.15 a.m.
[87] Joy D.C. (1991): The theory and practice of high-resolution scanning electron microscopy. *Ultramicroscopy*, 37, 216-233.
[88] Joy D.C, Pawely J.B (1992): High-resolution scanning electron microscopy. *Ultramicroscopy*, 47, 80-100.
[89] Agarwal P., Berglund K.A. (2004): Effect of polymeric additives on calcium carbonate crystallization as monitored by nephelometry. *Crystal Growth & Design*, 4, 479-483.
[90] Deluchat V., Bollinger J. C., Serpaud B., Caullet C. (1997): Divalent cations speciation with three phosphonate ligands in the pH-range of natural waters. *Talanta*, *44*, 897-907.
[91] Tomson M. B., Kan, A. T., Oddo J. E. (1994): Acid/base and metal complex solution chemistry of the polyphosphonate DTPMP versus temperature and ionic strength. *Langmuir, 10*, 1442-1449.
[92] Wiśniewska M., Urban T., Grządka E., Zarko V. I., Gun'ko V. M. (2014): Comparison of adsorption affinity of polyacrylic acid for surfaces of mixed silica–alumina. *Colloid and Polymer Science*, 292, 699–705.
[93] Chen K. M., Jiang X., Kimerling L. C., Hammond P. T. (2000): Selective self-organization of colloids on patterned polyelectrolyte templates. *Langmuir*, 16, 7825–7834.
[94] Miyazaki T., Yoshioka S., Aso Y., Kojima S. (2004): Ability of PPP and PAA to inhibit the crystallization of amorphous acetaminophen. *Journal of Pharmaceutical Sciences*, 93, 2710–2717.

[95] Dei L. Guarini G.G.T. (1997): The thermal decomposition of NaHCO3. *Journal of Thermal Analysis*, 50, 773–783.
[96] Xi, L. Fleet M. E. (2009): Phase relations of nahcolite and trona at high P-T conditions. *Journal of Mineralogical and Petrological Science*, 104, 25-36.
[97] Eugster H. P. (1966): Sodium carbonate-bicarbonate minerals as indicators of pCO_2. Journal of Geophysical Research71, 3369–3377.
[98] Thieme C. (1989): *Ullmann's Encyclopedia of Industrial Chemistry*. 5th Edition, American Chemical Society, Weinheim (Germany).
[99] Weast R. C. (1979) *CRC Handbook of Chemistry and Physics* (59th ed.), Boca Raton, Florida: CRC Press.
[100] Espinosa-Marzal, R. M. Scherer G. W. (2009): Advances in understanding damage by salt crystallization. *Accounts of Chemical Research*, 43, 897-905.
[101] Lide D. R. (2009): *CRC Handbook of Chemistry and Physics* (90th ed.). Boca Raton, Florida: CRC Press. ISBN 978-1-4200-9084-0.
[102] Ozaki, S. Kushida, I. Yamashita, T. Hasebe, T. Shirai, O. Kano K. (2013): Inhibition of crystal nucleation and growth by water-soluble polymers and its impact on the supersaturation profiles of amorphous drugs. *Journal of Pharmaceutical Sciences*, 102, 2273–2281.
[103] Mutaftschiev B. (2001): Equilibrium Between Large Phases; The Vapor Pressure of Solids. *The Atomistic Nature of Crystal Growth*. Springer Series in Materials Science, Springer, Berlin, Heidelberg, vol 43 pp. 43-60.
[104] Sikiric´ M., Babic´-Ivancˇic´ V., Milat O., Sarig S., Füredi-Milhofer H. (2000): Factors influencing additive interactions with calcium hydrogenphosphate dihydrate crystals. *Langmuir* 16, 9261–9266.
[105] Anthony J. W., Bideaux R. A., Bladh K. W., Nichols, M. C. (Eds.) (2003): *Handbook of Mineralogy*, Mineralogical Society of America, Chantilly, VA 20151-1110, USA. http://www.handbookofmineralogy.org/., volume V.
[106] Reynolds J.G, Huber H.J, Cooke G.A (2014): Solid-phase zirconium and fluoride species in alkaline zircaloy cladding waste at Hanford. *Journal of Hazardous Materials*, 278, 203-210.

Acknowledgements

Me gustaría que estas líneas sirvieran para expresar mi más profundo y sincero agradecimiento a todas aquellas personas que con su ayuda han colaborado en la realización del presente trabajo, en especial al Dr. Carlos Manuel Rodríguez-Navarro, director de esta investigación, por la orientación, el seguimiento y la supervisión continúa de la misma, pero sobre todo por la motivación y el apoyo recibido a lo largo de estos seis meses.

Especial reconocimiento merece el interés mostrado por mi trabajo y las sugerencias recibidas de la profesora Encarnación Ruiz-Agudo, por el ánimo infundido y la confianza en mí depositada. También me gustaría dar las gracias sinceramente a todos mis amigos y compañeros de trabajo del Departamento de Mineralogía y Petrología por acoger a esta extraña y hacerla sentir casi como española de verdad: Alejandro, Estefania, Nazaret, Cristina, Luis, Teresa, Agustín, Fulvio y Federica. Os espero en Sicilia!

Dopo sei mesi di *Spanglish* torno, con fatica, a scrivere in italiano.

I primi, e doverosi, ringraziamenti nella mia lingua madre vanno alla professoressa Elena Bernardi. Per la seconda volta si conferma mia relatrice e per la seconda volta non riesco a trovare poche e concise parole per esprimere la mia gratitudine nei suoi confronti. La ringrazio per la sua esperienza, la sua conoscenza, per la sua presenza costante e per la grande umanità con la quale ha saputo incoraggiarmi e supportarmi in tutti i momenti di difficoltà. La ringrazio perché per me più che una relatrice è stata una guida, una confidente e una saggia consigliera. Come al solito la ringrazio per aver fatto il suo lavoro con infinito amore. In qualunque posto la vita mi porterà, la porterò sempre nel mio cuore.

Ringrazio mia madre. La ringrazio per avermi insegnato a cavarmela ovunque e in qualunque circostanza. A Palermo, a Bologna, a Granada, senza paura e nonostante essa, con il sorriso o con un po' di rabbia, da sola o in compagnia. La ringrazio per il suo appoggio costante, perché mi spinge a puntare sempre più in alto senza aver paura di farmi male o fallire. Insomma, la ringrazio per avermi insegnato a vivere, a volare e a vedere il cielo azzurro oltre le nubi più scure.

L'ultimo ringraziamento va a Gioacchino. Ti ringrazio per tutte quelle volte che mi sei venuto a prendere ad una festa con la tua Vespa blu, per tutte le volte che tornando a casa

dall'ufficio mi hai portato un regalo, per tutte le volte in cui ho guardato uno di quei film che non sopportavi ma sei comunque rimasto seduto sul divano a vederlo con me. Ti ringrazio per avermi amata con quell'amore incondizionato che solamente i padri sanno dare ai loro figli, nonostante mio padre non fossi.

Mi sono rimproverata molte volte di non essere mai riuscita a ringraziarti di persona, ad esprimere a pieno quanto ti volessi bene e quanto fosse fondamentale la tua presenza nella mia vita. Ma tu tutte queste cose già le sai.

William Shakespeare diceva "all the world is a stage". Anche se il tuo tempo fra gli attori del mondo è finito, io ti vedo seduto in mezzo al pubblico, con gli occhiali sulla punta del naso e quell'immancabile sigaretta accesa, mentre ti godi lo spettacolo della mia vita.

E io mi impegnerò con tutte le mie forze per offrirti il più grande spettacolo che sia mai esistito.

Dal profondo del mio cuore, grazie infinite a tutti.